GENERAL ATOMIC

DIVISION OF GENERAL DYNAMICS

GA-7274

RADIATION EFFECTS ON LASERS

by

D. M. J. Compton and R. A. Cesena

TECHNICAL REPORT
July 1, 1965, through May 31, 1966

Contract NAS 12-32
National Aeronautics and Space Administration
Electronics Research Center
Cambridge, Massachusetts

September 21, 1966

GENERAL ATOMIC

DIVISION OF

GENERAL DYNAMICS

JOHN JAY HOPKINS LABORATORY FOR PURE AND APPLIED SCIENCE

P.O. BOX 608, SAN DIEGO, CALIFORNIA 92112

GA-7274

RADIATION EFFECTS ON LASERS

TECHNICAL REPORT
July 1, 1965, through May 31, 1966

Work done by:

D. M. J. Compton
R. A. Cesena
B. D. Kitterer

Report written by:

D. M. J. Compton
R. A. Cesena

During the period of this report, the following "reportable items" as defined by the article "Report of New Technology" evolved: None.

Contract NAS 12-32
National Aeronautics and Space Administration
Electronics Research Center
Cambridge, Massachusetts
General Atomic Project 521

September 21, 1966

Publications made during this contract period included two presentations to APS meetings:

"Effects of Irradiation on Optically Pumped Lasers"
by R. A. Cesena and D. M. J. Compton
Bull. APS, Series 11, 10, 1188 (1965)

and

"Irradiation of GaAs Laser Diodes"
by R. A. Cesena and D. M. J. Compton
Bull. APS, Series 11, 11, 714 (1966)

FOREWORD

This technical report "Radiation Effects on Lasers," was prepared by General Atomic Division, General Dynamics Corporation, San Diego, California under contract NAS 12-32 with NASA Electronics Research Center, Cambridge, Massachusetts. Research was carried out under the direction of Dr. D. M. J. Compton, the General Atomic Principal Investigator. The NASA Project Monitor was Mr. John Sullivan. The research reported herein was performed during the period July 1, 1965, through May 31, 1966.

ABSTRACT

This interim technical report describes the first part of a program to study the effects of space radiation on lasers. A discussion is given of the mechanisms by which these effects can occur, and of a suitable choice of parameters to be measured. These include "active" tests, such as output energy versus input energy and threshold plots; measurements of coherence and of near and far field patterns; and "passive" tests such as interferometric studies of optical perfection; optical transmission measurements; and scattering of transmitted gas laser light. Methods for measuring these parameters were developed and applied to optically pumped lasers such as ruby, $CaWO_4$:Nd, YAG:Nd and glass:Nd, and GaAs diode injection lasers, before and after irradiation with 32 Mev protons, 30 Mev electrons, and reactor γ rays. For the optically pumped lasers, a special cavity was developed which used external mirrors and could contain two laser rods in series, one pumped and one not: this cavity was used to show that the degradation produced by irradiation was due to optical loss. A simple theory of this optical loss is used to correlate the changes in threshold with changes in output power. Optical bleaching is found to be unimportant for the Nd-doped lasers, which are increasingly affected by radiation in the order YAG, $CaWO_4$ and glass. Dose-rate effects are very marked but can be explained by room temperature annealing processes, which were also studied using optical absorption. Annealing was also measured up to 300°C: electron damage is readily removed while proton damage is not. For GaAs diodes, irradiation does not change the current voltage curve, but degrades the optical output and changes the output wavelength spectrum. Coherence and far-field patterns are changed for all lasers if the input power is increased after irradiation to keep output power constant, and heating seems to be a more important cause of these changes than any direct effects of irradiation. The program is being continued.

CONTENTS

		Page
I.	INTRODUCTION	1
	1.1 Optical Effects of High-Energy Radiation	2
	1.2 Annealing of Radiation Effects	7
	1.3 Effects of Vacuum	8
	1.4 Dependence on Dose and Dose Rate	8
	1.5 Space Radiation	8
	1.6 Shielding	9
II.	CHOICE OF EXPERIMENTAL PARAMETERS	11
III.	APPARATUS AND METHODS	15
	3.1 Holder for Optically Pumped Lasers	15
	3.2 Holder for Semiconductor Lasers	24
	3.3 Coherence	27
	3.4 Near-field Patterns	41
	3.5 Far-field Patterns	43
	3.6 Optical Quality of Laser Rods Studied by Far-Field Pattern of Transmitted Gas-Laser Beam	43
	3.7 Light Scattering	51
	3.8 Interferometry	51
	3.9 Optical Absorption	51
	3.10 Apparatus to Run in TRIGA Reactor	51
IV.	RESULTS	57
	4.1 Output-input Curves on Optically Pumped Lasers	57
	4.2 Optical Bleaching	65
	4.3 Dose-rate Effects and Spontaneous Annealing	65
	4.4 Annealing	67
	4.5 Optical Absorption	67
	4.6 Effects of Different Types of Radiation	73
	4.7 Susceptibility to Radiation of Different Laser Rods	73
	4.8 Effects on GaAs Lasers	73
REFERENCES		75

FIGURES

		Page
1.	Laser assembly	16
2.	Triggering circuit for flashtube	18
3.	High-voltage charging supply	19
4.	Fast-response phototube circuit	21
5.	Detector and laser assemblies in position for laser output measurements	22
6.	Typical oscilloscope photographs of data taken with a $CaWO_4$:Nd laser	23
7.	A gallium-arsenide injection laser. The emitting face is the dark rectangle. Magnification is about 16	25
8.	Photograph showing the detector assembly and the cryostat. The injection laser is just visible through the Mylar window	26
9.	Circuit diagram of pulser for gallium-arsenide injection laser	28
10.	Circuit diagram of pulse train generator used for repetitive operation of injection laser	29
11.	Experimental arrangement used in the laboratory to measure the laser output of a GaAs injection laser	30
12.	Arrangement for measuring output spectrum of GaAs laser	31
13.	Spectra of GaAs injection laser before irradiation	32
14.	Spectra of GaAs injection laser after electron irradiation	33
15.	Dimensions of double slit used in coherence studies	37
16.	Experimental arrangement used in the laboratory to study coherence and near-field patterns. (For coherence studies, a slit is placed immediately in front of the shutter.)	39

FIGURES (Cont'd.)

		Page
17.	Diffraction patterns produced by coherent beam from a gas laser. (a) single slit, (b) double slit, (c) single slit illuminated with a GaAs injection laser	40
18.	Near-field patterns of a $CaWO_4$:Nd laser operated at (a) pumping energy of 7.9 J; (b) pumping energy of 6.2 J; and (c) pumping energy of 7.9 J after irradiation with γ rays. Total dose, 4,000 rads	42
19.	(a) Proton-induced coloration in a $CaWO_4$:Nd laser rod; (b) Laser near-field, showing absence of lasing or superradiance in irradiated area	44
20.	Experimental arrangement used to photograph far-field patterns	45
21.	(a) Far-field pattern of a $CaWO_4$:Nd laser rod; pump energy, 15 J; (b) transmitted beam of a gas laser, distorted by the laser rod. Note similarity to far-field pattern	46
22.	$CaWO_4$:Nd. (a) Far-field pattern of laser rod--pump energy, 17.5 J; (b) far-field pattern of transmitted gas laser beam	47
23.	Glass;Nd. (a) Far-field pattern of a transmitted gas laser beam showing good optical properties; (b) far-field pattern at slightly above threshold, 287 J; (c) far-field pattern at high pump power, 409 J	48
24.	YAG:Nd. (a) Far-field of a transmitted gas laser beam; (b) far-field pattern before irradiation, 30.2 J; (c) far-field pattern after irradiation with protons, 46.8 J	49
25.	Experimental arrangement used to study optical perfection	50
26.	Coloration produced by protons in (a) $CaWO_4$, (b) Al_2O_3, (c) borosilicate glass	52

FIGURES (Cont'd.)

		Page
27.	Water-tight cell used to measure laser output during gamma irradiation in TRIGA reactor	54
28.	Schematic showing internal arrangement of cell in Figure 27	55
29.	Circuitry used to measure ion chamber current	56
30.	Power output versus energy input for $CaWO_4$:Nd laser rod before irradiation	58
31.	Power output versus energy input for YAG:Nd before and after irradiation with gamma rays	63
32.	Power output versus pump energy for YAG:Nd laser before and after irradiation with protons. Degradation shows rapid spontaneous annealing. Dose: 5×10^9 protons/cm^2	64
33.	Power output versus irradiation time for a $CaWO_4$:Nd laser rod at constant pump energy; circles: 17.8 J; triangles: 31.0 J. Gamma dose rate versus irradiation time is shown by solid curve	68
34.	Recovery at room temperature of laser output from YAG:Nd rod following proton irradiation. Pump-lamp energy constant at 51.6 J. The final points are taken after 8 hr at 100°C	69
35.	Output from YAG:Nd laser rod before and after annealing for 8 hr at 100°C	70
36.	Optical density at 4, 100 Å of $CaWO_4$:Nd laser rod after γ-ray irradiation and annealing for 30 min at each of the indicated temperatures	71
37.	Decrease of optical density at 4, 100 Å of $CaWO_4$:Nd laser rod as a function of time at room temperature	72

I

INTRODUCTION

Lasers offer many potential advantages for space communications and space instrumentation. Their performance is, however, affected by the high energy radiation found in the space environment, e.g., trapped protons and electrons, solar flare protons, and possibly gamma rays and neutrons from on-board nuclear power, auxiliary or propulsive. The work reported here is the first part of a program intended to determine the vulnerability of lasers to such radiations, so that the seriousness of the problem can be assessed, and selection of optimum types can be made. In addition, the program includes studies of methods of combating the effects, such as shielding and annealing.

Three main types of lasers are now in use: optically pumped laser rods such as ruby, glass: Nd, or $CaWO_4$: Nd; gas lasers such as He : Ne or ion lasers; and p-n junction injection lasers such as GaAs diodes.

Several workers have studied the effects of high energy radiation on optically pumped lasers.

Flowers and Jenney[1] exposed ruby laser rods at temperatures of $\sim -130^{\circ}C$ to $\sim 10^6$ rads of γ irradiation from a Co^{60} source and found some evidence for a temporary increase in lasing output when rods are optically pumped to well above threshold. The increase in efficiency, as compared with the same rod without irradiation, diminished with successive flash-lamp pulses, a result which was attributed to the formation of color centers by the γ irradiation and their removal by the flash-lamp irradiation. These color centers, which were thought to increase the efficiency of absorption of pump light by the ruby, were removed by exposure to light or by heating. Other effects found included a change in the near-field output pattern of one rod, but no change in the relaxation oscillation pattern was detected. Johnson and Grow,[2] on the other hand, found that exposure of a ruby rod to $\sim 4 \times 10^4$ rads of Co^{60} γ rays caused an increase of $\sim 35\%$ in the lamp power needed to reach laser threshold. The lamp power at threshold increased with increasing γ-ray dose, but gradually decreased to the unirradiated value as the rod was lased a number of times. They also report a fivefold decrease in the luminescence of ruby after exposure to $\sim 10^6$ rads of Co^{60} γ irradiation. Davis et al.[3] report results generally similar to those of Flowers and Jenney,[1] with a doubling of laser output for a dose of ~ 1000 rads of Co^{60} radiation at room temperature. Low[4]

describes some features of the coloration of ruby by x rays and postulates an effect in increasing laser output when using flash lamp pumping, as had Gabrysh et al.[5] Smith[6] reported on an experiment in which a ruby laser could be operated at ~100°F during and after insertion into a high powered (30 MW) reactor. Experimental problems were very severe, and laser and flash lamp output had to be monitored thermally, using thermocouples. These problems made it difficult to reach quantitative conclusions. In general, laser output was markedly decreased, with perhaps a tendency to a somewhat smaller decrease at higher reactor powers. However, laser operation was apparently possible during an exposure lasting a few seconds at $\sim 1 \times 10^5$ rads sec^{-1} (reactor γ rays).

In the report literature, workers at Martin-Orlando[7] have given a descriptive outline of some of the effects that might occur, together with some other measurements that are not immediately relevant to the present problem. A rather similar outline was given by Davis, et al.[8] The work of Johnson and Grow was also published as a report.[9]

At General Atomic, detailed studies have been made of the effects of pulsed high-intensity irradiation on the output of ruby, $CaWO_4$: Nd, and glass : Nd lasers. This work appears in the proceedings of a classified conference[10] and a portion of it has been published[11].

No work has apparently been performed on the effects of radiation on gas lasers. It is to be expected that moderate dose rates of high-energy radiation would only slightly perturb the ionization and excitation already present in the gas discharge, and thus no effects would be produced. Very high dose rates of electrons have been shown[12] to cut off laser action in certain lines of a noble-gas ion laser, but dose rates expected from space radiation are expected to affect only auxiliary components of a gas laser, such as the windows, the reflective coatings used as mirrors, and modulation equipment (e.g. electro-optical crystals).

Injection diode lasers are directly susceptible to radiation, as are most other semiconductor components. Measurements on GaAs diode lasers have been reported briefly by Saji and Inuishi[13]; it is not clear from their work that the devices they made were really acting as lasers. A number of workers[14, 15, 16] have studied radiation effects on GaAs electroluminescent diodes.

1.1 Optical Effects of High-energy Radiation

High-energy irradiation can introduce many changes in the optical properties of materials. These include the introduction of optical absorption from color centers, the change of optical emission due to valence

change of emitting ions, and the introduction of light scattering and changes of refractive index. In semiconductors, the optical emission efficiency can be decreased and optical absorption introduced.

It is useful to divide the mechanisms of introduction of these effects into two classes: ionization radiation effects and displacement radiation effects. The first class is associated with excitation and deexcitation of electrons due to ionization and can be produced by low-energy radiation such as soft x rays, low-energy electrons, or even energetic ultraviolet photons. Typical mechanisms by which ionization effects cause changes in optical properties are:

a. Trapping of electrons or holes produced by the radiation in defect centers, which may already be present or produced by irradiation. The classic examples are the F centers in the alkali halides. Because of their disordered structure, glasses are very subject to this mode of coloration, which can often be produced by ultraviolet light.

b. Change of valency of an impurity ion by capture of a hole or electron. Examples include substitutional aluminum in quartz,[17] which is responsible for much of the coloration, and rare-earth ions in laser crystals. In the latter case, irradiation is often used to effect a desired valence change.

Changes in optical properties, resulting from irradiation, are attributed to ionization effects, even when their detailed mechanism is unknown, if they can be produced by low-energy radiation and if they can be reversibly removed by optical bleaching or mild thermal treatment (see below). A typical case of this kind is provided by changes in absorption in quartz.[18] The magnitude of ionization radiation effects is determined by the ionization energy deposited in the sample, and for equivalent doses and dose rates is essentially independent of the nature and energy of the radiation. The equivalence of electrons, fast protons, and γ rays (interacting via electrons produced) when compared in this manner is well established, and ionization energy deposition rates by various types and energies of radiation are known reasonably well. Neutrons (interacting chiefly via knocked-on atoms) deposit relatively little energy as ionization in nonhydrogenous materials.

Displacement radiation effects are associated with the displacement of atoms from their lattice sites. They result from a close collision of a fast particle with the nucleus of an atom, giving the atom enough energy to displace it from its lattice site. Typical mechanisms by which displacement

effects produce optical changes include:

a. Introduction of defect levels in the forbidden gap of an insulator. Optical absorption can then take place by excitation of an electron from the center to the conduction band or to a higher excited state of the center, or of an electron from the valence band to the center. Since electronic excitation is involved, the observation of optical absorption will depend upon whether the levels involved are full or empty of electrons. Cases of this kind include vacancies in MgO,[19] and many centers in semiconductors;

b. Broadening of the band edge, extending the optical absorption to longer wavelengths. This effect is well known in many semiconductors;

c. Introduction of light scattering from disordered regions produced by energetic interactions (fast neutrons or "stars" from high-energy protons);

d. Perturbation of the selection rules in a crystal near a defect, thus shifting the wavelength of a transition. An example is the α center in alkali halide crystals.

Displacement radiation effects are very sensitive to both the type and the energy of the radiation concerned. The displacement properties of atoms in a solid can be characterized reasonably well for a given material by the threshold energy below which an atom will not be displaced. Hence, for a fast nuclear particle to cause a displacement, it must have a minimum threshold energy, which will depend upon the mass of the particle and the mass of the struck nucleus. Following the initial displacement, the displaced atom may move through the material and collide with other atoms, displacing some of them until all of the displaced atoms come to rest; this mechanism causes defects in the material. These defects, including vacant sites and interstitial atoms, may then migrate, either at the irradiation temperature or upon annealing at a higher temperature. This process may result in the annihilation of the defect, or in the formation of a complex defect with an impurity atom already present in the material.

For the case where the fast nuclear particle is an electron, displacements are produced by the Coulombic (Rutherford) interaction between the electron and the atomic nucleus, with a cross section independent of electron energy for relativistic electrons (>1 MeV). The distribution function of the energy E of the primary recoil atom in a Coulombic collision is proportional to E^{-2}, so that most of the recoil atoms produced have low energies. The total number of displaced atoms can be roughly estimated by dividing the

energy of the primary displaced atom by twice the atomic displacement threshold energy. Electrons with energy of approximately 1 to 2 MeV thus tend to displace only one atom and form simple defects, while collisions of higher energy electrons (5 to 50 MeV) result in an average displacement of several atoms and may give different, more complicated, aggregate defects.

For protons, Coulombic (Rutherford) scattering is also the chief mechanism for producing defects at low energies (< about 20 MeV). Since protons in this energy range are nonrelativistic, the cross section for Rutherford scattering decreases with increasing proton energy as 1/E, a result which is confirmed experimentally. Low-energy protons are thus responsible for most of the displacement-effects damage in the unshielded space environment, but effective shielding is possible.

At higher proton energies (but beginning at ~10 MeV), it is necessary to allow for the effects of nuclear elastic scattering; i.e., scattering involving the short-range nuclear forces, rather than the Coulombic interactions. This additional contribution can be estimated fairly accurately using the optical model of the nucleus and the numerous experiments on various elements; the cross sections vary only slowly with atomic number. At higher proton energies, nuclear inelastic processes (nuclear reactions) are also important. These add to the cross sections and change the momentum of recoil atoms. Protons with energies greater than ~100 MeV may produce another mode of interaction: nuclear "star" production. This spallation reaction is violent enough to produce a marked effect on the number of displacements produced, in spite of a rather low interaction cross section (~1 b for 500-MeV protons). This extra effect can be considered as two mechanisms: (1) The production of lower energy "star secondary" nucleons. These produce additional displacements and are relatively more effective than the primary protons because the protons of have higher scattering cross sections and the neutrons have a more effective interaction mechanism. (2) Displacement of atoms by the recoiling residual nucleus; this may displace a very large number of atoms before coming to rest.

Calculations made at General Atomic indicate that (1) in comparison with the primary beam, the star secondaries can be neglected, (2) because the recoiling nucleus produces several thousand displacements, this process has a considerably higher over-all efficiency of displacement production than all other processes involved in star reactions combined.

Another mechanism for the production of displacement effects is interaction with fast neutrons. This process causes large numbers of displaced atoms per event and is thus somewhat similar to nuclear star production. Neutrons are not an important part of the natural space

environment, but will of course be important in a vehicle carrying a nuclear reactor. This displacement effect of fast neutrons arises because the interactions between an incident fast neutron and a nucleus are via the nuclear force field, which is both stronger and of shorter range than the Coulombic interaction. This leads to a smaller cross section, but also to an approximation of a hard-sphere collision in which a large fraction of the maximum possible energy is transferred in an average collision. With neutron energies near 1 MeV, a target nucleus of medium mass will receive several tens of kilo-electron-volts; this will result in a total of several thousand displaced atoms per primary collision. High-velocity recoils will also lose a substantial amount of energy as ionization.

Thermal neutrons are effective in producing damage only if they can produce a nuclear reaction. An important case is with boron-containing laser glasses, where the $B^{10}(n, \alpha)$ reaction, which has an enormous cross section and yields high-energy recoil fragments, gives very great sensitivity to thermal neutrons.

Simulation of the displacement effects of space radiation thus needs careful consideration of electron and proton energies and flux, since exact duplication is not possible. Establishment of correlation among proton, electron, and neutron damage rates at various energies has been under theoretical and experimental study at General Atomic for Ge and Si.[20]

For Ge, the calculations predict, for 30-MeV proton, a defect-introduction rate of 20 times that for 30-MeV electrons. For carrier-removal and lifetime changes on samples with a variety of dopings, the measured values range from 13 to 40.

A third mechanism for formation of defects is, in a sense, intermediate to the above two. Ionization effects in some materials can result in the displacement of atoms. This is well known in the formation of color centers in alkali halides. Continued formation of F centers involves the displacement of negative ions to leave vacancies, but displacements can be achieved with radiation that cannot cause them directly, e.g., 50-kV x rays. The detailed mechanism is still uncertain, but may involve an Auger effect or the energy of electron-hole recombination.[21] The process is of a typically ionization type, e.g., work at General Atomic has shown that equal F-center generation is produced by soft x rays or by 30-MeV electrons depositing the same ionization energy. This process is very important for alkali halides, and it has recently been suggested that it may be somewhat important in the III-V semiconductors of which typical injection lasers are made.

These mechanisms differ greatly in their relative efficiencies for producing optical effects. For example, if expressed in terms of the number of electron volts needed on the average to form a defect (although this is not really a fair method of presentation), optical absorption introduced by ionizing processes will require only a few electron volts. An example is the initial range of coloration of KCl, where approximately 80 eV are required per F center formed. Ionization-type processes leading to displacement of atoms, such as the later stages of coloration of KCl, require of the order of 1000 eV per F center. Displacement effects of a fairly simple nature, as, for example, those produced by 4.5-MeV electrons in Si, require, when expressed in these terms, approximately 1.5 MeV per defect.

1.2 Annealing of Radiation Effects

The radiation effects, once introduced, are apt to disappear in several ways. One is by thermal annealing. Annealing of this kind occurs for virtually all types of radiation damage, and often in a series of discrete steps as the temperature is raised. Annealing of this kind has been reported specifically for ruby.[1-5]

Many optically absorbing centers introduced by irradiation can be bleached by optical illumination, a process known as optical bleaching. A classic example is the F center in alkali halides. This process has been reported for ruby. The process is of great importance to the present program, since measurements of laser action after irradiation necessarily involve intense illumination. The damage produced by previous irradiation may thus be completely or partially lost, and the damage may then no longer be assumed to be cumulative. In certain cases, ultraviolet light from the flash lamp can serve to introduce electrons and introduce additional coloration, which is, in a sense, inverse optical bleaching. Solarization of glass from this cause is well known.

A third mechanism of annealing is caused by the high electric fields in p-n junction devices, which can cause defects to migrate and thus change the properties.[21] This may be important in GaAs diodes.

It should be mentioned that optical bleaching, and certain types of thermal bleaching, may remove the coloration from a crystal, but may not leave it in the state it was in before irradiation. Specifically, irradiation may produce vacancies in a material via displacement effects. These may be filled with electrons and absorb light. Optical bleaching may remove these electrons, but leave the vacancies. The vacancies can then be refilled by any type of ionizing radiation, not necessarily one capable of producing displacement effects, so that the crystal is now much more readily colorizable.

1.3 Effects of Vacuum

Many oxide and tungstate materials show enhanced colorizability when irradiated in vacuum. This is associated with loss of oxygen. An oxygen atom is lost from the surface, which, in the crystal, had been an $0^{=}$ ion. There are two electrons left in the crystal, which enter sites and form color centers. Since they are mobile, the coloration can occur throughout the bulk of the crystal. This effect is most marked with radiation of low penetration, such as soft electrons, ultraviolet photons, etc., but should be considered in the present application.

1.4 Dependence on Dose and Dose Rate

Many of the effects described above are expected to depend on the total radiation dose administered and on the dose rate used.

Optical effects need to be measured as a function of the dose given to the sample because the function cannot be assumed to be linear. A typical form for the curve of concentration of optically absorbing centers versus total radiation dose has an initial rapidly increasing portion followed by a more slowly rising portion. In some materials, a saturation of the optical absorption is seen; in other cases a decrease is observed at high doses. The saturation effects may arise from the finite concentration of an impurity necessary to form the center or from radiation annealing. A decrease may also be due to radiation annealing or to changes in the electronic occupation of the center being observed.

Variation of optical absorption with the rate at which the dose is administered is also a common occurrence and may arise whenever competing processes are involved. A particular example is afforded by the infrared-absorbing complex defect centers in alkali halides, the M and N centers which are aggregates of F centers. The ratio of M to F centers has been found[23] to depend on the dose rate and type of radiation used to form the defects. Work at General Atomic[24] has shown the mechanism of this effect. When pulsed irradiation is used, the destruction of M centers induced by radiation is found to depend on a higher power of the dose rate than their formation. Thus they are formed at low dose rates and are destroyed at high dose rates.

1.5 Space Radiation

The space radiation environment consists of trapped-particle belts, (electrons and protons), solar flares (high-energy protons), galactic cosmic rays (protons, some α particles, and other nuclei), and solar-wind protons. Electrons and protons are the only components of importance, and it is assumed that all uv photons will be filtered or shielded out. The fluxes

involved will not be further discussed here, as they have been extensively treated in numerous references (e.g., 25, 26, 27).

1.6 Shielding

Shielding from space radiation has also been very extensively studied.[28, 29, 30] An important factor is the build-up of bremsstrahlung in the shields used, since this is much more penetrating than the original electron or proton flux.

II

CHOICE OF EXPERIMENTAL PARAMETERS

In a program of this type, it is necessary to choose carefully the experiments to be performed, since exact simulation of the space environmental effects on a large number of lasers cannot be achieved. It is desirable to obtain not only data of direct interest to the systems designer or engineer who may have to select a laser for a particular application, but also a basic scientific understanding of the processes occurring, so that the results obtained can be extrapolated to other systems than those actually measured.

Typical laser types were selected from both the optically pumped and injection-diode categories. From the first were chosen ruby (because of the extensive studies already made on this material), $CaWO_4$:Nd, glass : Nd, and YAG : Nd (yttrium aluminum garnet). These last three are typical well-studied low-threshold materials, and have Nd in common as the active ion. From the second category, GaAs laser diodes were obtained from various manufacturers.

The radiation sources used were chosen to simulate the important components of the space radiation environment. 32-MeV protons represent penetrating protons which will displace several atoms in a typical collision, and show the effects of nuclear elastic scattering. Gamma-rays are used to represent the brehmsstrahlung produced by electron or proton impact on shielding used. Thirty-MeV electrons are used as a convenient source of penetrating radiation that can be related to the 32-MeV protons,[20] and also shows good agreement with the predicted damage rates at other electron energies.

The source of protons used was the 32-MeV-proton linear accelerator at the University of Southern California. The machine delivers an average current of $\sim 10^{-8}$ amp of 31.5-MeV protons in 450-μsec pulses at a repetition rate of 15 per sec.

The γ-ray source was one of the TRIGA reactors at General Atomic, used to deliver mixed γ-rays which are given off for some time after shutdown following reactor operation. For very low dose rates, a 40-Ci source of Cs^{137} was used to deliver about 100 rads/hr to a sample.

The 30-MeV electrons were obtained from the General Atomic Electron Linear Accelerator, which gives pulses of electrons with energies from 4 to 45 MeV.

Other types of radiation that will be used later in the program, when reliable measurements have been made with the above, include 1-to 3-MeV electrons from the General Dynamics/Convair Dynamitron Accelerator and neutrons from the TRIGA reactor.

The experimental program involves the selection of suitable parameters for measurement. These fall into two clases, active and passive. Active tests include such quantities as

a. threshold pump power,

b. laser output versus power input,

c. coherence, and

d. beam divergence and near- and far-field patterns.

Passive tests, mostly applicable to optically pumped lasers, include

a. optical absorption of a laser rod,

b. scattering index, e.g., measuring the transmission of a gas laser through the rod to study how much light is scattered out of the beam in passing through the rod, and

c. studies of optical perfection, using interferometry.

Once suitable means have been developed for measuring these parameters, the effect of high-energy radiation on them can be studied, as can the effect of sample treatments, such as annealing.

"Active" tests of laser performance have the advantage of testing the operationally important parameters of the laser. For example, irradiation may introduce color centers which add to the absorption of pump light and increase the nonuniformity of temperature during optical pumping, thus increasing beam divergence. Similarly, if irradiation lowers the output power of a laser, active tests are necessary at the original output-power level, obtained by increasing input power, to determine how badly the coherence is affected by the higher heating produced. Passive tests, however, have the possible advantages of being nondestructive; e.g., it may be possible to avoid complications due to optical bleaching (see below) and to give data which is important to reaching an understanding of the effects occurring.

It is also necessary to evaluate two possible complicating effects. The first is optical bleaching, which can complicate interpretation of results by removing an uncertain fraction of the effects produced by irradiation every time the laser is optically pumped. Similar effects appear to occur with electrical bleaching of GaAs laser diodes. The second is dose-rate

and annealing effects at the temperature of irradiation and measurement. If the effects produced depend on the dose rate at which a given dose of radiation is delivered, or on time between irradiation and measurement, they must be carefully evaluated in order to obtain any meaningful measurements as well as to enable correlations to be made to the low dose rates of the space environment.

Most of the work reported here involves the development of methods for obtaining reliable measurements of these parameters, and these methods will be described in the following section.

III

APPARATUS AND METHODS

This section of the report describes the special apparatus and methods developed to measure the parameters listed above, and the effects of irradiation, and subsequent annealing, on them.

3.1 Holder for Optically Pumped Lasers

Optically pumped crystal or glass laser rods use an optical cavity with reflective ends to establish laser oscillation and directionality. The end mirrors (typically multidielectric layers) may be planar or confocal, and a choice must be made between two methods of assembly that have many operational differences. One has the mirrors evaporated directly onto the end faces of the laser rod, which are polished to be plane parallel or confocal as desired. The other uses separately mounted mirrors with the rod placed between them. The ends of the rod are given antireflection coatings. The first method has the advantage of providing low threshold, so that smaller effects of irradiation can be seen; of providing a laser output independent of small variations in the position of the rod; and of being the method that would probably be used in operational use of a laser. This method has the problem, however, that the nearly 100%-reflecting coatings on the laser rod preclude many 'passive' measurements on the rod, such as studies of optical transmission or optical quality. Nevertheless, it is possible to make some of these measurements, if desired, at wavelengths where the coatings are not 100% reflective. The second method has the advantage that the rod coatings are nonreflective, so that passive measurements may be readily made. In addition, if this type of optical cavity is made with the distance apart of the mirror being 2-3 times the rod length, threshold is increased, but the mode structure of the laser output is greatly simplified. Lasers of this type emit from only one or a few filaments that are active at any one time, and selection of one or a few such filaments makes measurements of coherence simpler. It also makes it possible to place other optical elements inside the optical cavity. For example, one (unpumped) laser rod can be placed inside the cavity formed by the end mirrors and another (pumped) laser rod. The effects of losses in the first laser rod can then be studied under conditions where it is not being optically pumped.

The apparatus used on this program was designed to allow either mode of operation and is shown in Figure 1. Two flat and parallel dielectric

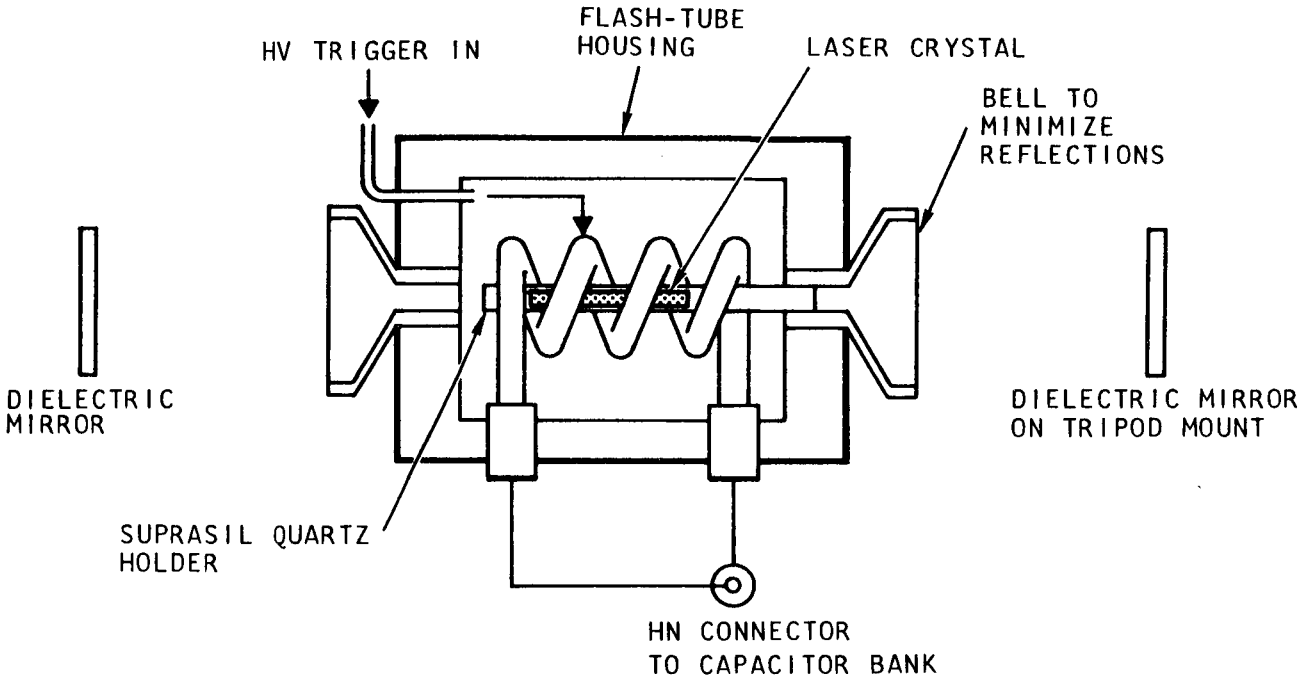

Fig. 1--Laser assembly

mirrors used to form the cavity have reflectivities of 95% and 99%. They are mounted in Fabry-Perot etalons with a spacing of 30 cm. These etalons, which can tilt the mirror plane along two axes by means of differential screws, are mounted rigidly on a large bar of heat-treated steel.

The laser rod, which may, if desired, have its ends coated to minimize reflections, is now mounted in a special fixture concentric with the flashtube. This fixture is a tube of very high purity fused synthetic quartz (Suprasil*), which holds the crystal as a slip fit and allows the crystal to be removed and replaced with only a small error in axial position.

The flashtube used is a xenon-filled, helical lamp 3/8 in. id and 2 in. long. A helical flashtube is used because linear flashtubes tend to pump different lengths of a laser rod as the power to the flashlamp is increased, instead of increasing the inversion level of the whole laser rod. The flashlamp is held inside the aluminum housing by boron nitride supports, which also provide electrical insulation and chemical resistance to the high-intensity flash. Triggering is accomplished by inducing a discharge inside the flashtube by a high-voltage pulse applied to a tight-fitting nickel sleeve surrounding the flashtube helix. (The sleeve also serves as a light reflector.) The high-voltage pulse, typically 25 kV, is generated using an EGG TR-60 transformer and associated pulsing circuitry, shown in Figure 2. The flashtube housing has provision for gas cooling, if desired.

Power to the flashtube is delivered through RG-8 cable from a bank of capacitors whose value of capacitance is chosen and placed in the circuit by a heavy-duty rotary switch. To shape the pulse into one with a more-desirable longer duration, an EGG TR-71 choke is included in series in the circuit. Charging voltage is supplied by a variable dc power supply whose schematic is shown in Figure 3, and which can be controlled to ±1 V. The voltage across the capacitors is monitored using a Kintel digital voltmeter to read the voltage across a calibrated voltage divider. With this arrangement, capacitor voltages, and therefore energy supplied to the flashtube, are chosen easily and with good reproducibility.

The light emanating from a laser is characterized by a number of very fast relaxation spikes of extremely high intensity. The use of a standard photomultiplier tube to observe and measure these pulses has serious limitations:

a. High optical density attenuators, usually several together, are necessary to keep the tube from saturating. These are difficult to calibrate.

---

*(Suprasil, TM Engelhard Industries. This type of fused silica is not significantly affected by the radiation doses used in this program.)

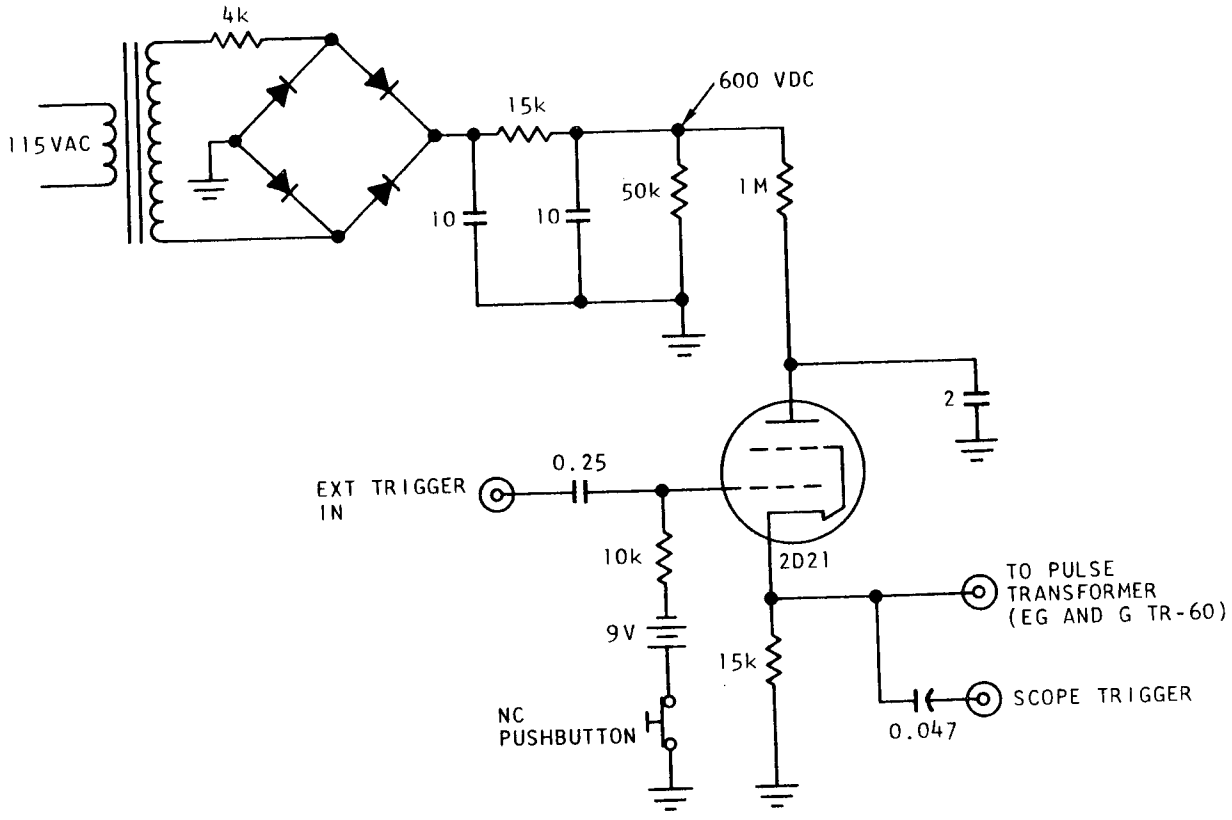

Fig. 2--Triggering circuit for flashtube

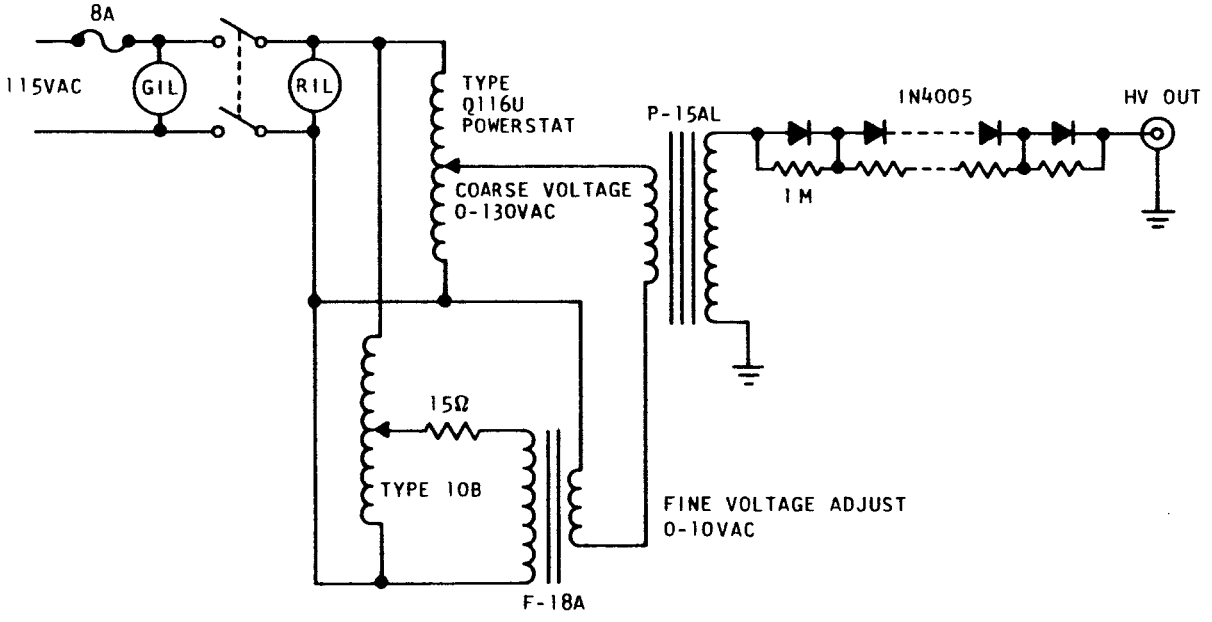

Fig. 3--High-voltage charging supply

b. The transit time of the electrons sets an upper limit to the response time of the detector.

c. For most tubes, the output current must be kept low to avoid exceeding the range over which the tube output is linear with input. This leads to low signals which need amplification and a cathode-follower to drive a terminated cable. The low output signals also lead to difficulties with noise currents produced in cables by the flashlamp discharge.

Accordingly, the photodetectors used were planar photodiodes of the FW-4000 series, manufactured by ITT. These are available with an S-1 photoresponse, so that they are usable at the 1.06 μ output wave length of Nd lasers, and are characterized by extremely fast response and by being linear over a wide range of output, up to several amperes. Typical voltages applied to the tube are 1000 to 5000 V. The diode is enclosed in a metal shell, which is grounded and shaped to provide an impedance match with General Radio GR-874-series 50-Ω plumbing. To provide the heavy currents required, a special high-voltage 0.01-μF capacitor is enclosed in a specially designed fitting. The capacitor also provides the necessary high-voltage isolation for decoupling the high voltage from the measuring oscilloscope. A schematic of the detector circuit is shown in Figure 4. The output of the diode is transmitted to the measuring oscilloscope through terminated 50-Ω cable. This provides the fast response necessary for proper evaluation of laser pulses. A photograph of the optical cavity-photodiode assembly is shown in Figure 5. A narrowband interference filter is generally used to pass the laser wavelength of interest and exclude pump light from the photodetector. The components are rigidly mounted to an aluminum beam, so that they can be moved readily from laboratory to accelerator. The ion chamber mounted next to the flashtube is used to monitor γ-ray dose rates (see below).

The output from the photodiode signal is divided between two channels of a Tektronix type-551 dual-beam oscilloscope. One channel is used to display on the upper trace of the scope the laser emission versus time. The signal sent to the second channel is electronically integrated with one section of a Tektronix type-O operational amplifier plug-in unit and is then amplified with the second section of the unit. This is necessary when measuring low laser output, e.g., near threshold. The integrated and amplified signal is sent to the second channel of the scope, which is generally a type-L high-gain preamplifier plug-in, in the lower beam section of the scope. Figure 6 shows typical oscilloscope photographs: The top picture shows the form of the laser output from a low-energy input to the flash lamp, and the lower picture shows that from a high energy input. Results are processed by measuring the amplitude of the lower trace, which is the integrated signal;

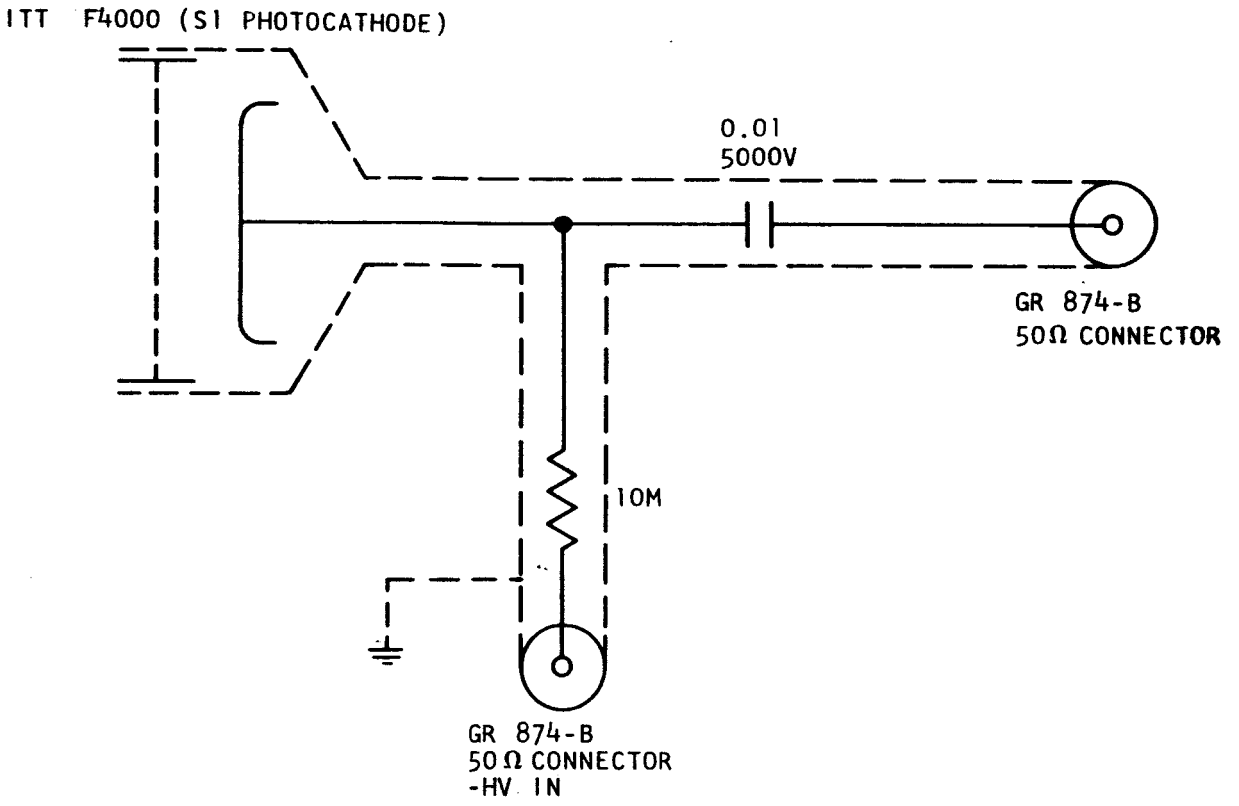

Fig. 4--Fast-response phototube circuit

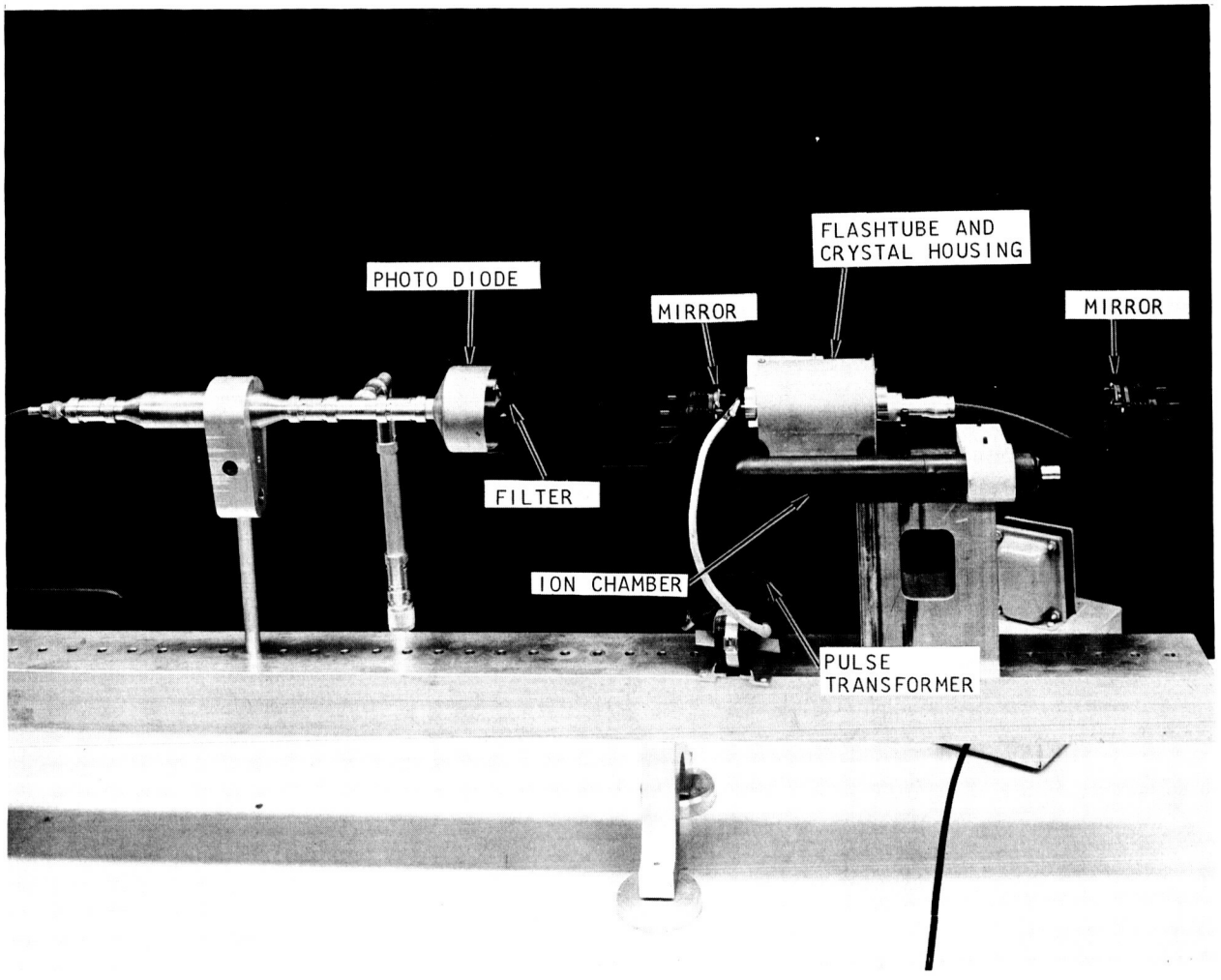

Fig. 5--Detector and laser assemblies in position for laser output measurements

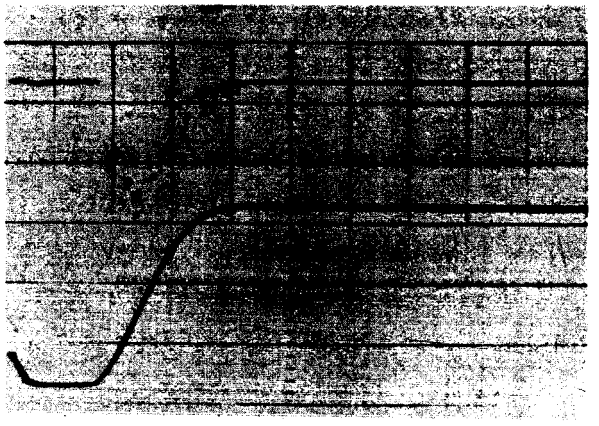

Pumping energy: 10.8 J
Upper trace: Laser output;
Gain, 1 V/cm
Lower trace: Integrated
laser output;
Gain, 0.02 V/cm

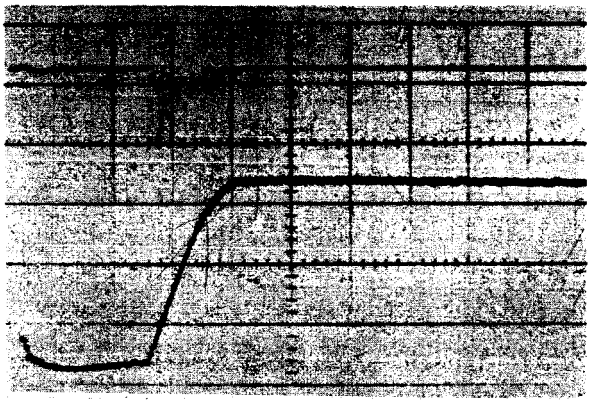

Pumping energy: 16.2 J
Upper trace: Laser output;
Gain, 1 V/cm
Lower trace: Integrated
laser output;
Gain, 0.1 V/cm

Fig. 6--Typical oscilloscope photographs of data taken with a $CaWO_4$:Nd laser

multiplying by the appropriate gain; and manipulating the calculated voltage output, using the relation

$$e_{out} = -\frac{1}{RC}\int e_{in}\, dt \ ,$$

where the limits of integration are found by the duration of the laser output pulse as presented by the upper trace of the picture. The output in volts is proportional to the energy received by the phototube and depends on many variable factors such as laser-detector separation and alignment, calibration of the photodetector, etc.; therefore, only arbitrary units are used to represent the laser output power. This is satisfactory, since only changes are of interest, and reproducibility of the photodetecting system has proved satisfactory.

A typical measurement of interest is the output energy versus input energy of the laser. To do this, the integrated output is plotted as a function of the energy stored in the capacitor bank immediately before firing the laser, as derived from the voltage indicated by the digital voltmeter.

The repetition rate is kept sufficiently low that heating effects are avoided. If necessary, gas cooling may be used, and gas can be admitted to the flashlamp housing for this purpose. The gas used should be clean air, as it was found that N_2 gas gave a laser output dependent on gas-flow rate. This was found to be associated with partial loss of the flashlamp energy to the nitrogen gas. Presumably, the electron attachment of the oxygen in air is sufficient to prevent this effect, which is much worse in helium.

3.2 Holder for Semiconductor Lasers

Semiconductor injection lasers need to be excited with high-current short pulses and, generally, to be cooled to 77°K. A typical laser is shown in Figure 7. To study the effects of irradiation, a special cryostat was constructed; it is shown in Figure 8. It is made of stainless steel, and is evacuated with a liquid nitrogen cooled molecular-sieve pump, so as to avoid vibration from mechanical pumps and to make it readily portable. To admit the high-energy radiation, windows of 0.0005-in. Mylar are used. These do not degrade or scatter protons appreciably and allow viewing of the diode. The radiation strikes the diode at right angles to the plane of the junction. The laser radiation exits from the cryostat through a thin Suprasil or sapphire window. The diode is pulsed by the circuit shown in

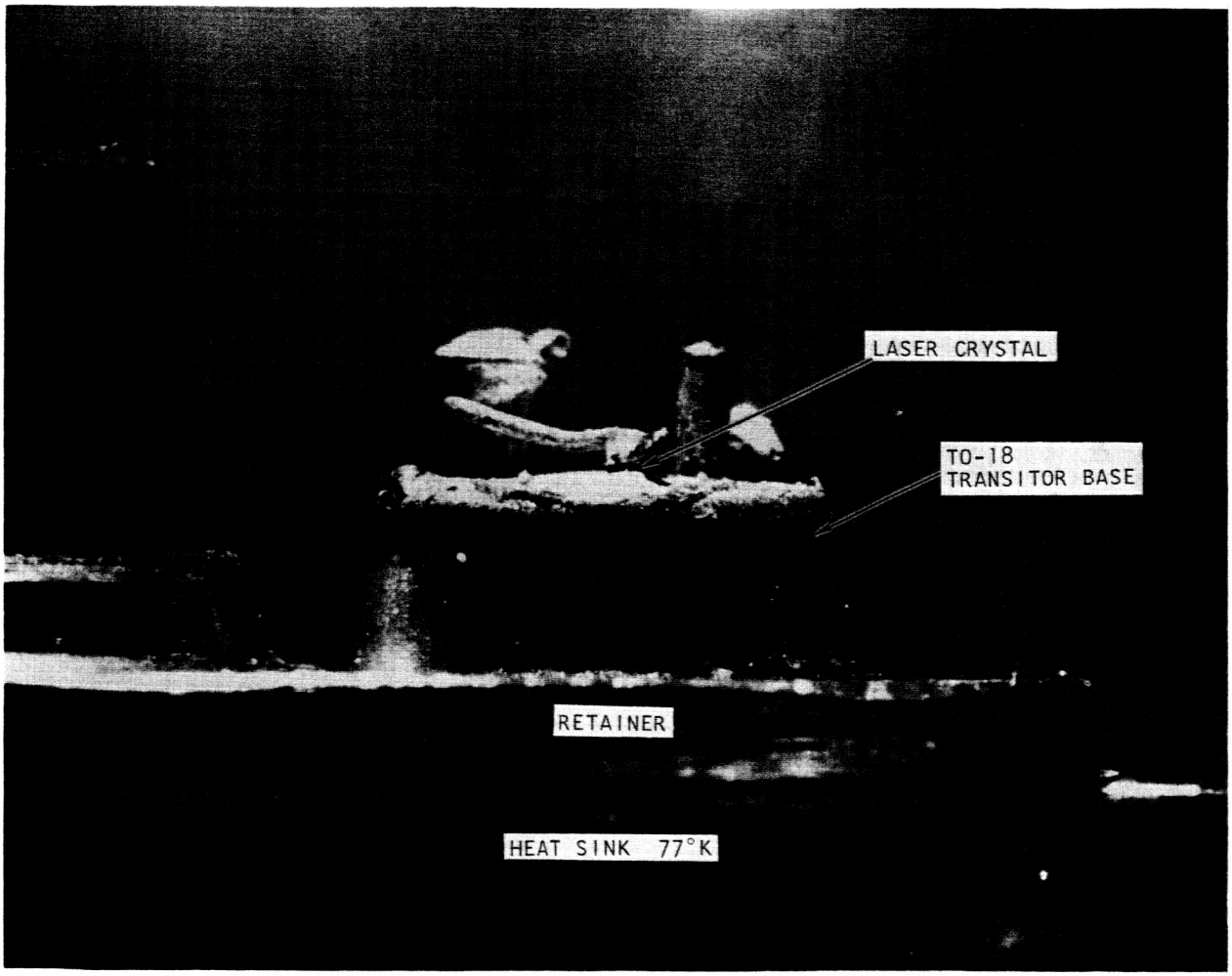

Fig. 7--A gallium-arsenide injection laser. The emitting face is the dark rectangle. Magnification is about 16

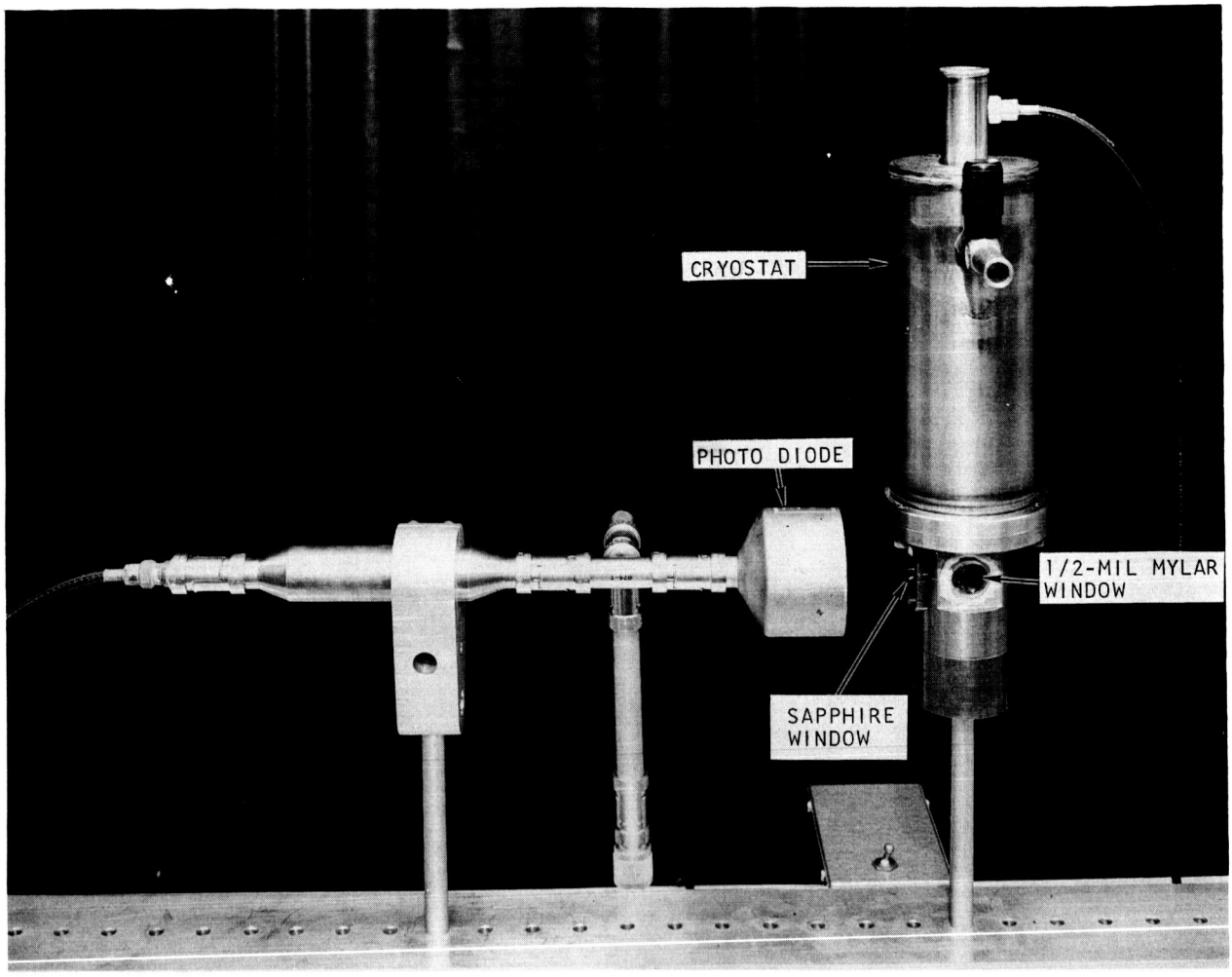

Fig. 8--Photograph showing the detector assembly and the cryostat. The injection laser is just visible through the Mylar window

Figure 9 and can be single pulsed, or can be pulsed repetitively by using the trigger generator shown in Figure 10. The pulser is a simple capacitor, thyratron, discharge circuit, using an R-L loop to shape the pulse into an approximate sinusoid of 2-μsec half-width.

The current in the pulse can be adjusted as desired by varying the charging voltage applied to the capacitor. This charging voltage is read to ± 1/2 V with a Kintel digital voltmeter. The magnitude of the injection current is measured by a Tektronix CT-2 current transformer incorporated in the diode circuit. It provides a voltage output across a 50-Ω termination which is directly proportional to the current and which remains linear for currents up to 100 amperes.

The laser optical output is monitored using an ITT FW4000-S1 planar photodiode, as described above. No filter is necessary to exclude pump light. The terminated output of the photodetector is fed into a Type L preamplifier, which then presents it on one of the traces of the dual beam oscilloscope. The output of the current monitor is displayed on the other trace and represents the injection level. The laser output is then plotted as a function of the injection current. Figure 11 shows the general experimental arrangement.

To study the effects of radiation on the spectral emission properties, the GaAs laser, in its cryostat, is mounted on the optical axis of a Jarrel-Ash Ebert 3.4-m plane grating spectrograph using a 15,000 lines-per-inch grating. Figure 12 shows the cryostat mounted on the accessory bar of the spectrograph. The photographic plates used are 4 × 10 glass-based Kodak emulsions I-N and IV-N. Figures 13 and 14 show the spectra of a GaAs injection laser before irradiation and after electron irradiation. A new lower energy level produced by the irradiation is quite distinct. Wavelength, as checked by the Ar reference lines, increases from right to left.

3.3 Coherence

The usefulness of a laser for long-distance communication depends upon its properties of coherence and directionality. Changes in these can be more serious than reductions in output power produced by irradiation. Measurements of coherence are thus of great interest but are somewhat difficult.

The theory of coherence, which is essentially a description of an average quantity of an electromagnetic field, involves the function $\Gamma_{12}(\tau)$ where

$$\Gamma_{12}(\tau) = \langle V_1(t + \tau)\, V_2^*(t) \rangle \quad ,$$

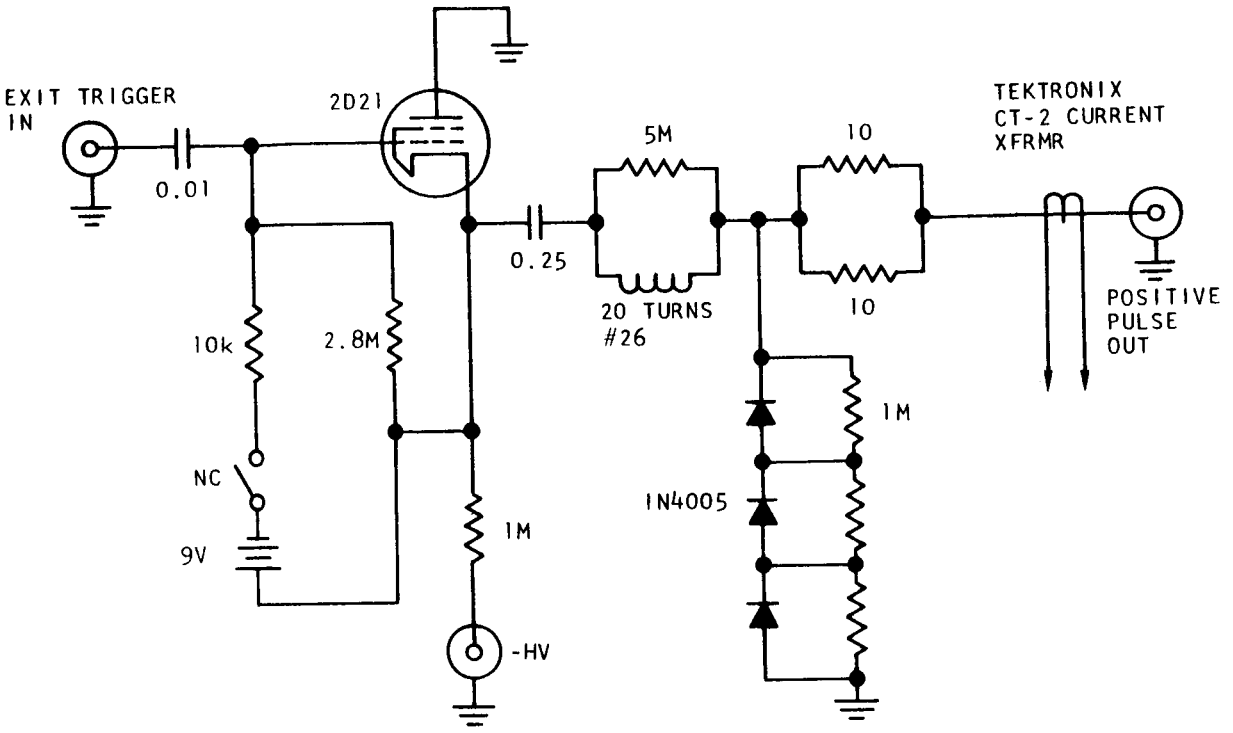

Fig. 9--Circuit diagram of pulser for gallium-arsenide injection laser

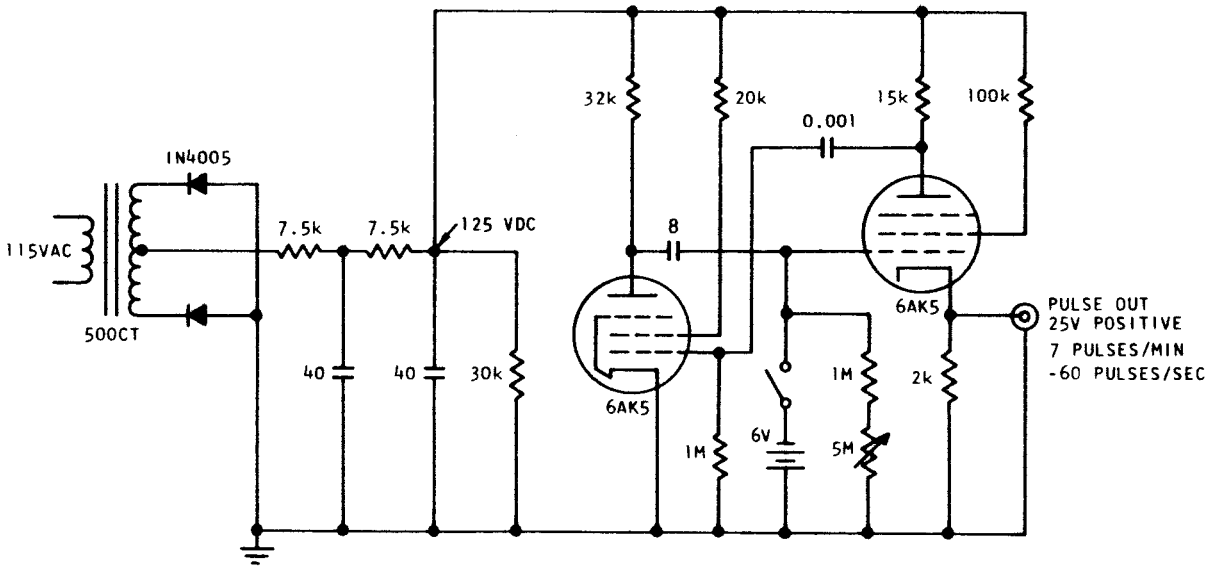

Fig. 10--Circuit diagram of pulse train generator used for repetitive operation of injection laser

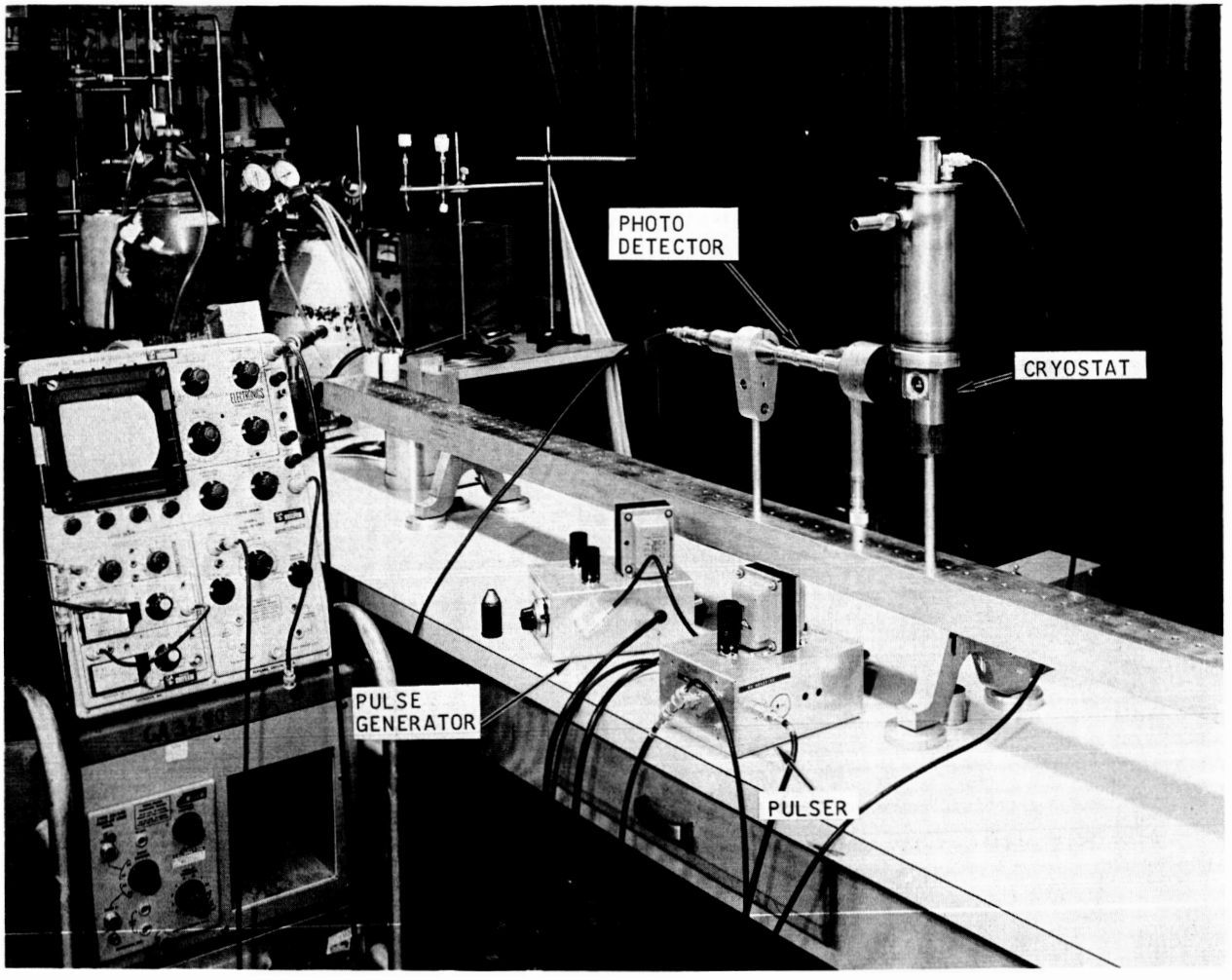

Fig. 11--Experimental arrangement used in the laboratory to measure the laser output of a GaAs injection laser

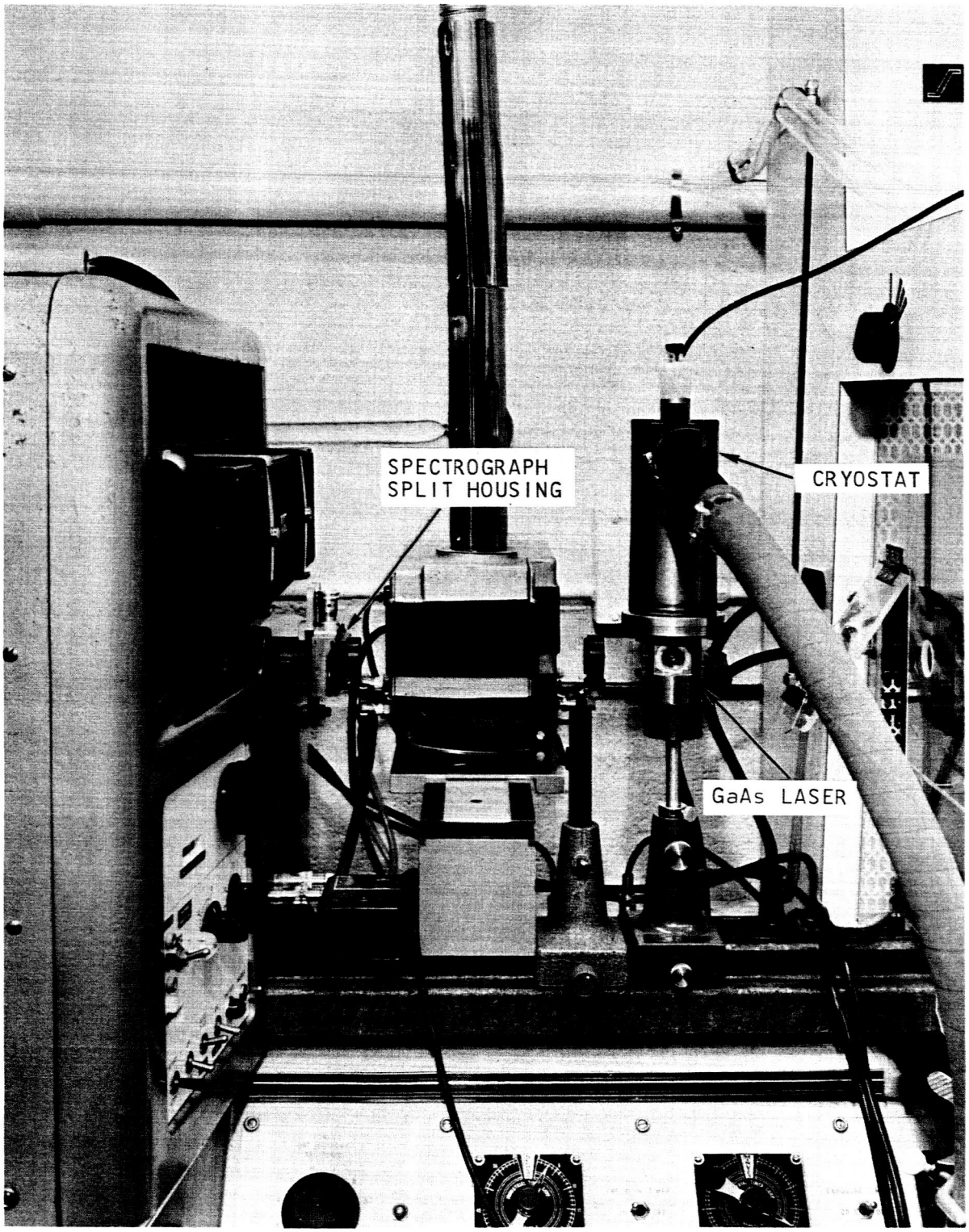

Fig. 12--Arrangement for measuring output spectrum of GaAs laser

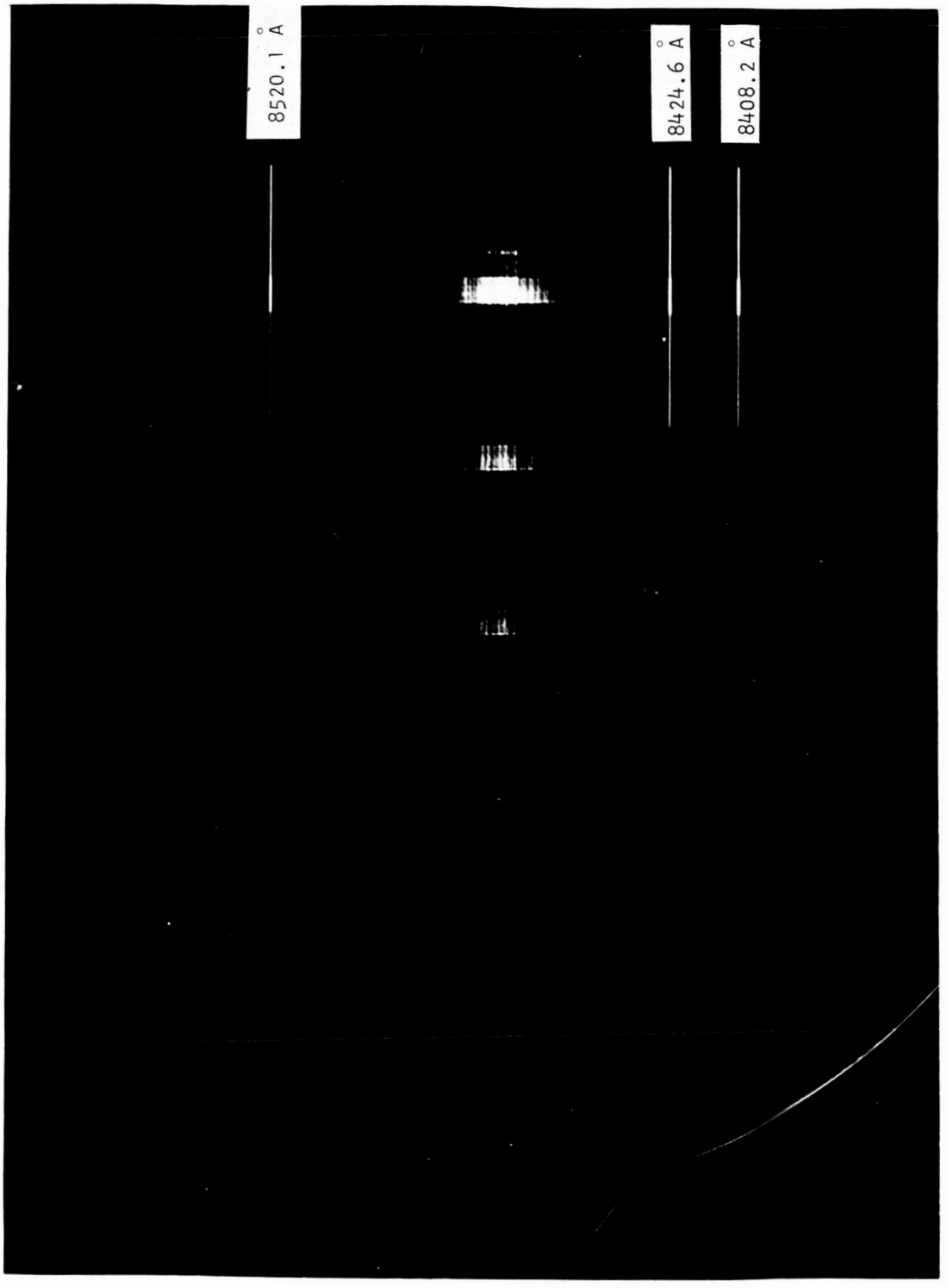

Fig. 13--Spectra of GaAs injection laser before irradiation

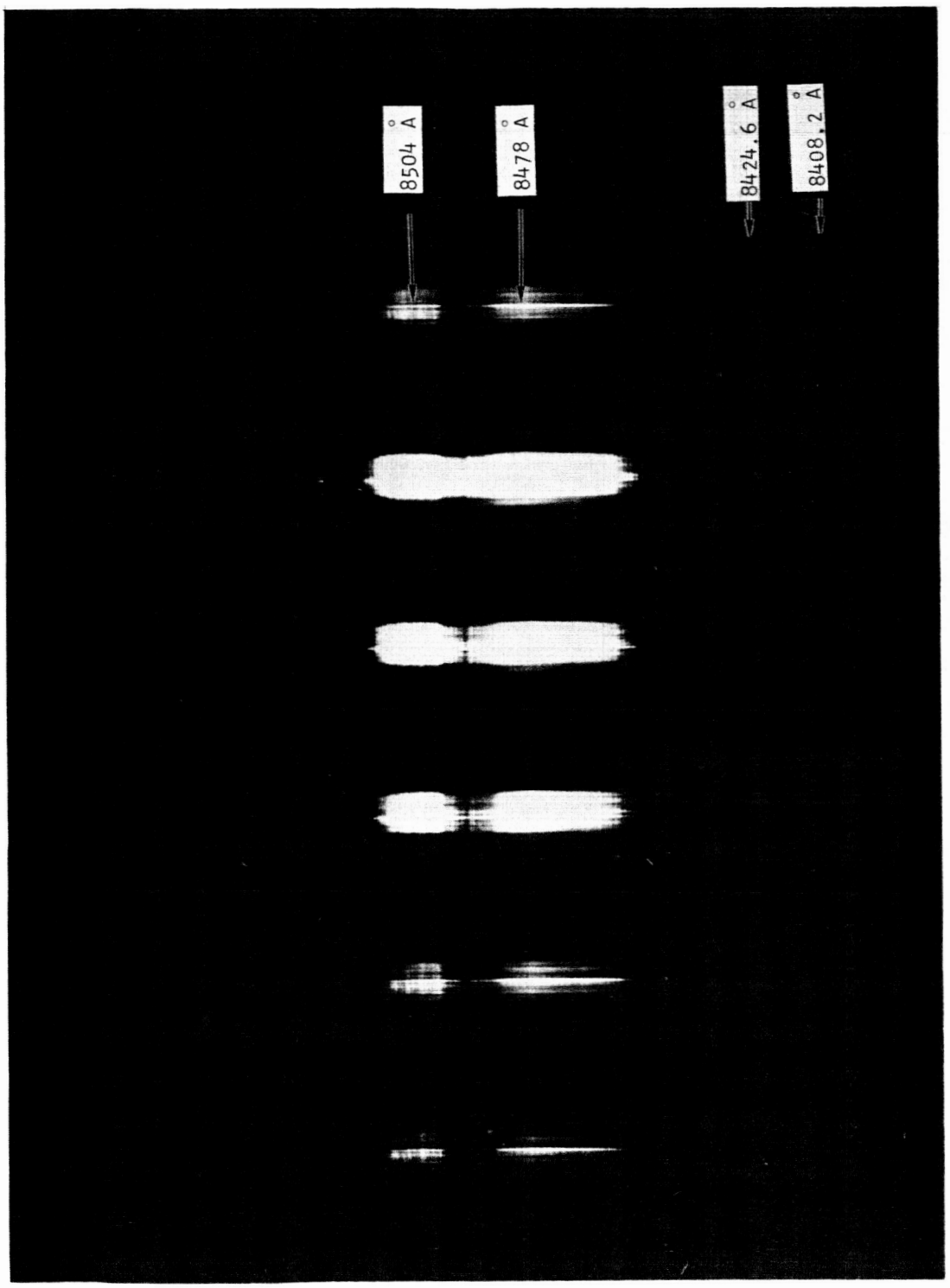

Fig. 14--Spectra of GaAs injection laser after electron irradiation

as described in detail in Beran and Parrent,[31] and is called the mutual coherence function. Its normalized form

$$\gamma_{12}(\tau) = \frac{\Gamma_{12}(\tau)}{\left[\Gamma_{11}(0)\right]^{\frac{1}{2}}\left[\Gamma_{22}(0)\right]^{\frac{1}{2}}}$$

is called the complex degree of coherence of the electromagnetic field and can be shown to have the limits given by

$$|\gamma_{12}(\tau)| \leq 1 \quad .$$

When $\gamma_{12}(\tau) = 1$, the field is said to be coherent; when $\gamma_{12}(\tau) = 0$, the field is said to be incoherent. Laser fields are generally partially coherent.

The usual method of measuring coherence follows the classical double-slit experiment of Young. In this experiment, a source illuminates an opaque plane which contains two small slits or holes. The intensity distribution on a second plane on the far side of the apertures is viewed with some appropriate sensing device. It is observed that if the illuminating field is partially coherent, interference effects will take place and manifest themselves in the form of intensity fluctuations on the viewing plane. Following the development in Born and Wolf,[32] the intensity at some point p on the observing plane is given by

$$I(p) = I_1(p) + I_2(p) + 2\left[I_1(p)\right]^{\frac{1}{2}}\left[I_2(p)\right]^{\frac{1}{2}}\left|\gamma_{12}(\tau)\right| \cdot \cos\left[\alpha_{12}(\tau) - \delta\right]$$

where

$I_1(p)$ = intensity at p due to one aperture alone,

$I_2(p)$ = intensity due to the second aperture alone,

$\gamma_{12}(\tau)$ = degree of coherence of the radiation illuminating the apertures,

$\alpha_{12}(\tau)$ = phase factor associated with the radiation, and

δ = phase difference between $I_1(p)$ and $I_2(p)$.

The time delay τ is best described by

$$\tau = 1/c \left[S_2(p) - S_1(p)\right] \quad ,$$

where S_1 is the path length from aperture 1 to the observing point p, and S_2 is that between aperture 2 and p. δ then becomes

$$\delta = 2\pi\bar{\nu}\tau \quad ,$$

where $\bar{\nu}$ is the mean frequency.

It might be noted at this point that $\alpha_{12}(\tau)$ describes the property known as temporal coherence, but this will not be followed further here.

Maxima and minima will be observed, to a good approximation, corresponding to

$$I_{max} = I_1(p) + I_2(p) + 2\left[I_1(p)\right]^{\frac{1}{2}}\left[I_2(p)\right]^{\frac{1}{2}}|\gamma_{12}(\tau)| \quad ,$$

$$I_{min} = I_1(p) + I_2(p) - 2\left[I_1(p)\right]^{\frac{1}{2}}\left[I_2(p)\right]^{\frac{1}{2}}|\gamma_{12}(\tau)| \quad .$$

Using the term "visibility" introduced by Michelson to describe the distinctness of the maxima and minima,

$$V = \frac{I_{max} - I_{min}}{I_{max} + I_{min}} = \frac{2\left[I_1(p)\right]^{\frac{1}{2}}\left[I_2(p)\right]^{\frac{1}{2}}|\gamma_{12}(\tau)|}{I_1(p) + I_2(p)} \quad .$$

From the above relation, it can be seen that if the apertures are illuminated uniformly, $I_1(p) = I_2(p)$, and $V = |\gamma_{12}(\tau)|$. However, if the illumination is not uniform, we must measure the intensities $I_1(p)$ and $I_2(p)$ in order to determine $|\gamma_{12}(\tau)|$.

It can be seen that the qualitative effects of partial coherence, namely interference, can be demonstrated readily in the laboratory. A source of light can thus be examined for coherent properties, but the determination of the exact degree of coherence is considerably more difficult.

The difficulty with lasers lies not only in the fact that they emit in short pulses with multimoding, but in the fact that emission can take place at random over the laser face. With low threshold lasers such as YAG:Nd and $CaWO_4$:Nd, the output can be reduced to just above threshold so that only one or two filaments emit; this is not possible with glass:Nd or ruby, which prefer to emit with many modes or none at all.

Several investigators[33] have shown that the laser emission takes place from small diameter (0.05 cm) filaments, whose number is dependent on the pumping energy. Each filament has been shown to be highly coherent. If the diffraction slits are illuminated by a number of such filaments, the visibility of the observed fringes deteriorates and the long time averaged coherence is small. A similar deterioration occurs if the slits are illuminated unevenly, as by a single filament slightly off the axis of the system.

The effects of nuclear radiation on $\Gamma_{12}(\tau)$ are expected, by virtue of the nature of stimulated emission, to be either intrinsically small and difficult to measure or absent.

A number of attempts were made to use the double-slit system, but they foundered chiefly on the difficulty of illuminating both slits equally when the laser would emit from one filament of unpredictable location. The double slit had the dimensions shown in Figure 15. After considerable effort, this method was abandoned in favor of a single-slit method.

Parrent and Skinner[34] have analyzed the diffraction patterns produced by a single slit illuminated with light of varying degrees of coherence. Their results show that coherent light produces an intensity pattern following a sine-squared function and noncoherent light produces a pattern obeying a cosine-squared function. The concept of the visibility of fringes can be used here, not to measure the degree of coherence but to look for small changes in coherence.

The single-slit experiment is easier to perform because it is relatively insensitive to misalignment and provides an image of higher

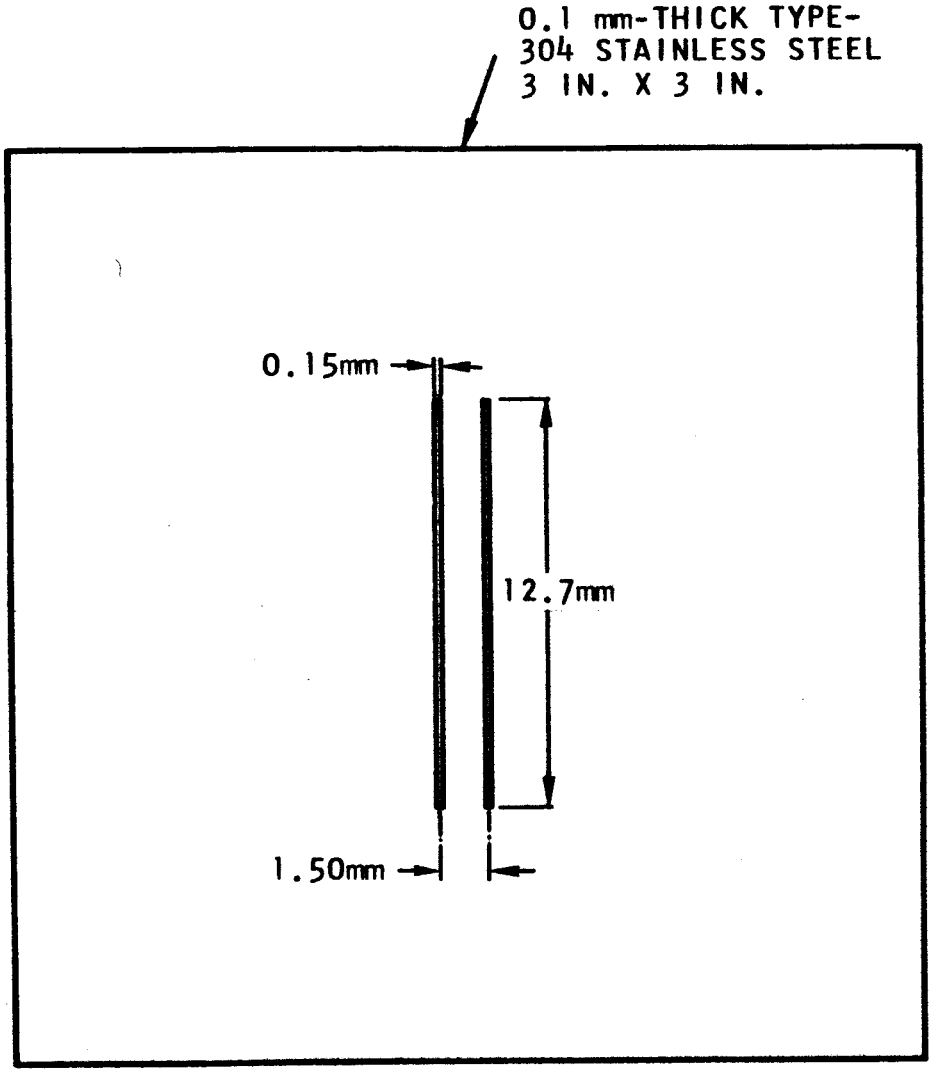

Fig. 15--Dimensions of double slit used in coherence studies

intensity. The technique used in this laboratory employs a single slit similar in dimensions to one of the pair shown in Figure 15. The slit, which is mounted on a vernier cross slide, is aligned to the axis of an optically pumped laser by passing a small-diameter beam of light from a gas laser through the rod and adjusting the slit until the first-order fringes are equal in brightness. Alignment of a GaAs injection laser is achieved by the reverse process, i.e., passing the beam from a gas laser through the slit and adjusting it until the zeroth-order fringe appears centered on the emitting face of the laser crystal.

The experimental arrangement is shown in Figure 16. A camera body (4 X 5 Calumet bellows type) is used to hold the film; the lens is removed, and the slit is placed immediately in front of the shutter. The shutter is used to keep out stray light and is opened for a little longer than the laser emission. The laser-to-slit separation is 15 cm, and the slit-to-film plane is 12 cm. The interference pattern is recorded on glass plates to prevent warpage and minimize shrinkage. The plates are developed with continuous agitation in D-19 developer for a standard 5 min, fixed in Kodak fixer containing a hardener, and washed in running water for at least 5 min, with a final rinse in distilled water. The plates are then air dried. The plates are scanned using a Jarrell-Ash scanning densitometer which records the density on a strip chart. The densities as measured on the chart must be corrected for the nonlinear nature of photographic emulsions, i.e., the H and D curve. This is done by standard spectrographic techniques.

Figure 17(a) shows a diffraction pattern obtained with a single slit illuminated with a gas laser. Misalignment shows up as an unequal brightness of opposite corresponding fringes. Figure 17(b) shows a double-slit experiment with the gas laser beam and slit axis misaligned to approximately the same extent as in (a), or about 0.01 cm from the position giving a single central maximum. Figure 17(c) shows the diffraction pattern of a single slit when illuminated with a GaAs injection laser. Four diffraction orders are visible on the original plate.

Other problems arise with optically pumped lasers. First, the pump light emerging from the end of the rod tends to expose the film. This effect is magnified by the much greater sensitivity of the film to the blue pump light than to the red or infrared emission from a ruby or Nd-doped laser. If a narrow-band filter is used to eliminate the pump light, it produces interference patterns of its own. The best way to overcome this seems to be to increase the distance between laser and slit, so as to preferentially attenuate the noncollimated pump light. Second, the only photographic materials that can be used at the Nd wavelength (1.06 μ) are so insensitive that it is not possible to obtain an image with a single spike output.

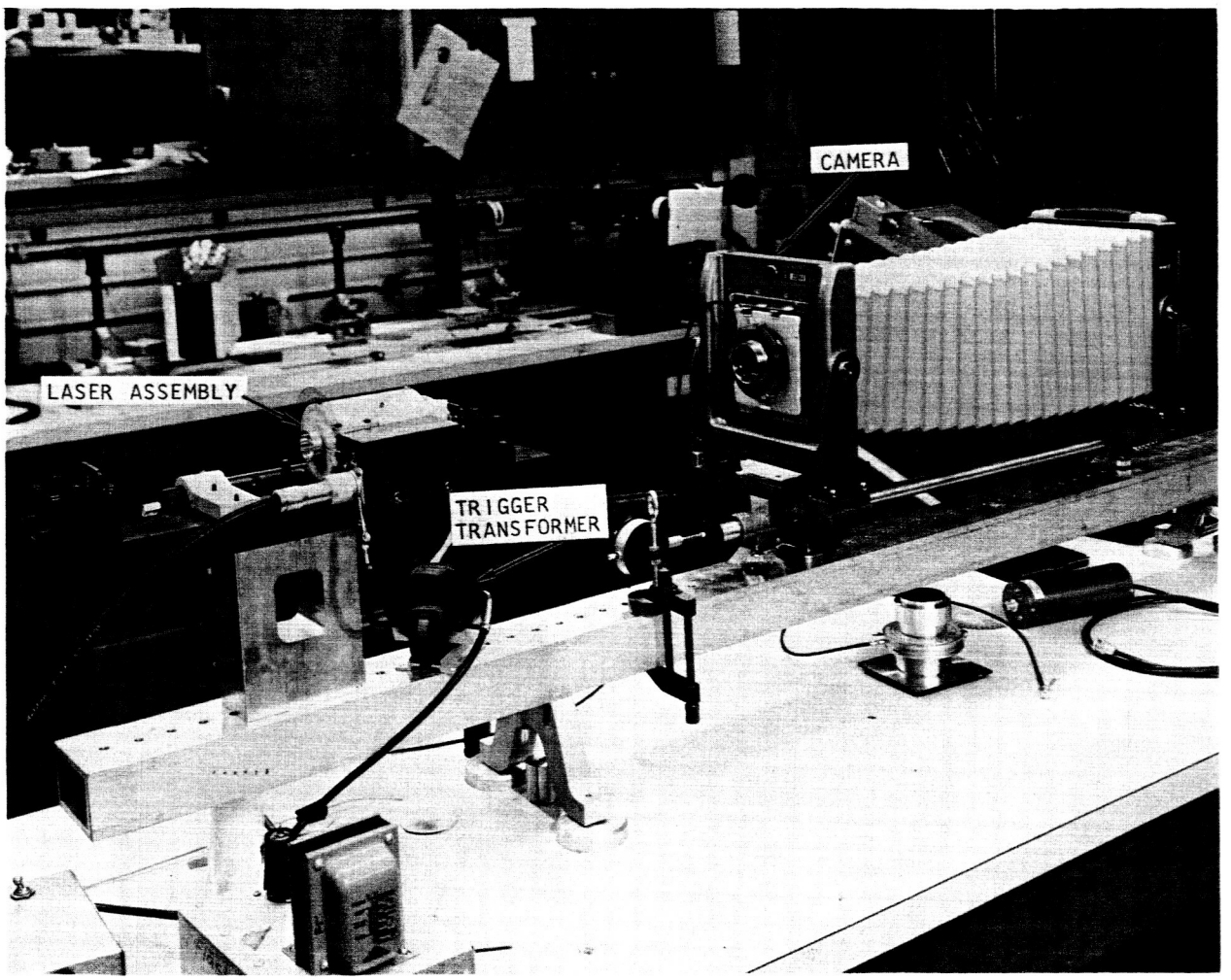

Fig. 16--Experimental arrangement used in the laboratory to study coherence and near-field patterns. (For coherence studies, a slit is placed immediately in front of the shutter.)

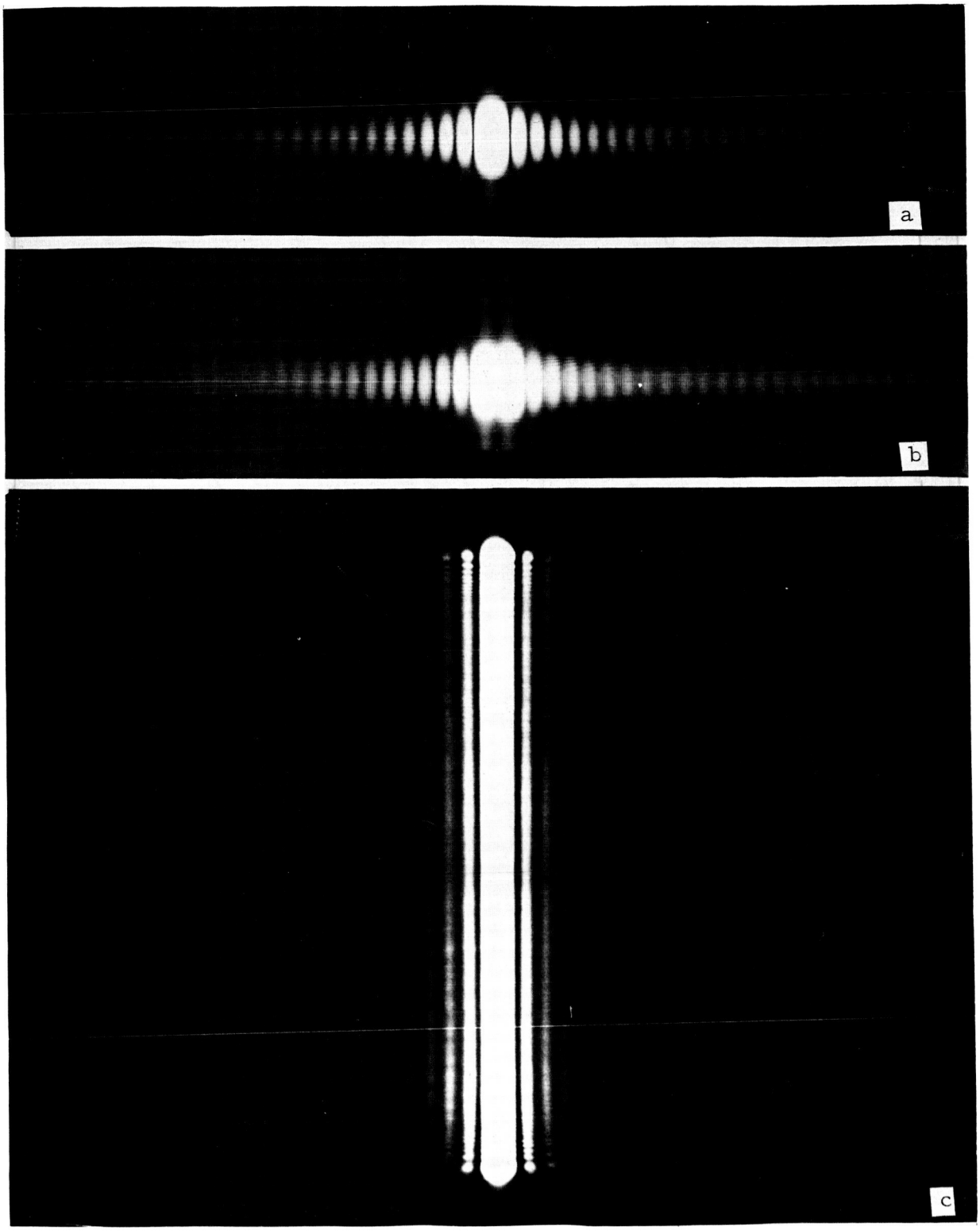

Fig. 17--Diffraction patterns produced by coherent beam from a gas laser. (a) single slit, (b) double slit, (c) single slit illuminated with a GaAs injection laser

3.4 Near-Field Patterns

Photographic studies have shown that laser emission takes place from small-diameter filaments whose number is a function of the pumping power and the Q of the cavity. These studies have examined the property of a laser which is termed "near field" or Fresnel field. It is simply the intensity distribution of emission sites on the face of the crystal. A photograph of the near-field pattern will show the size and location of any filaments that have emitted during the pulse. At pumping energies at threshold, or just above, the emitting filaments are quite distinct, but as the pump power increases to larger values, superradiance tends to obscure the filaments.

The technique used to measure the near-field patterns is illustrated in Figure 16. The camera is used fully extended. Several lens assemblies are available, but for near field photography, a 90-mm f/8 Schneider lens is preferred, which gives a fivefold magnification of the object at the film plane. Because the depth of field is very small at these short focal distances, careful focussing is necessary, and a small correction must be made for any movement of the focus caused by a change from visible to infrared light or by the introduction of a filter. This readjustment is made most conveniently by observing the linear motion of the camera assembly with a dial indicator. For example, this motion is 0.011 cm from the visible focus for 10,600 Å light when a particular infrared filter is used to exclude pump light; the original setting is found by trial and error. Eastman Kodak glass plates are preferred for laser emission studies because they are stable and will not wrinkle or warp. The emulsions used are shown in Table I. Polaroid 4 x 5, type 47 and type 55 p/n film is used for some optical studies and in general alignment procedures.

Table I

EASTMAN KODAK EMULSIONS

Device	Emission Wavelength (Å)	Emulsion Type
He-Ne gas laser	6,328	103a-F
Ruby	6,943	103a-F
GaAs injection lasers	8,400	I-N;IV-N
$CaWO_4$:Nd; YAG:Nd	10,600	I-Z

Figure 18 shows three typical near-field photographs of the emission from a $CaWO_4$:Nd rod. Figure 18(a) shows the filament structure of the laser at a pumping level of 7.9 J; (b) shows the structure at a level of 16.2 J and the appearance of superradiance. The ring-shaped pattern outlines the outside surface of the rod and is not caused by pump light.

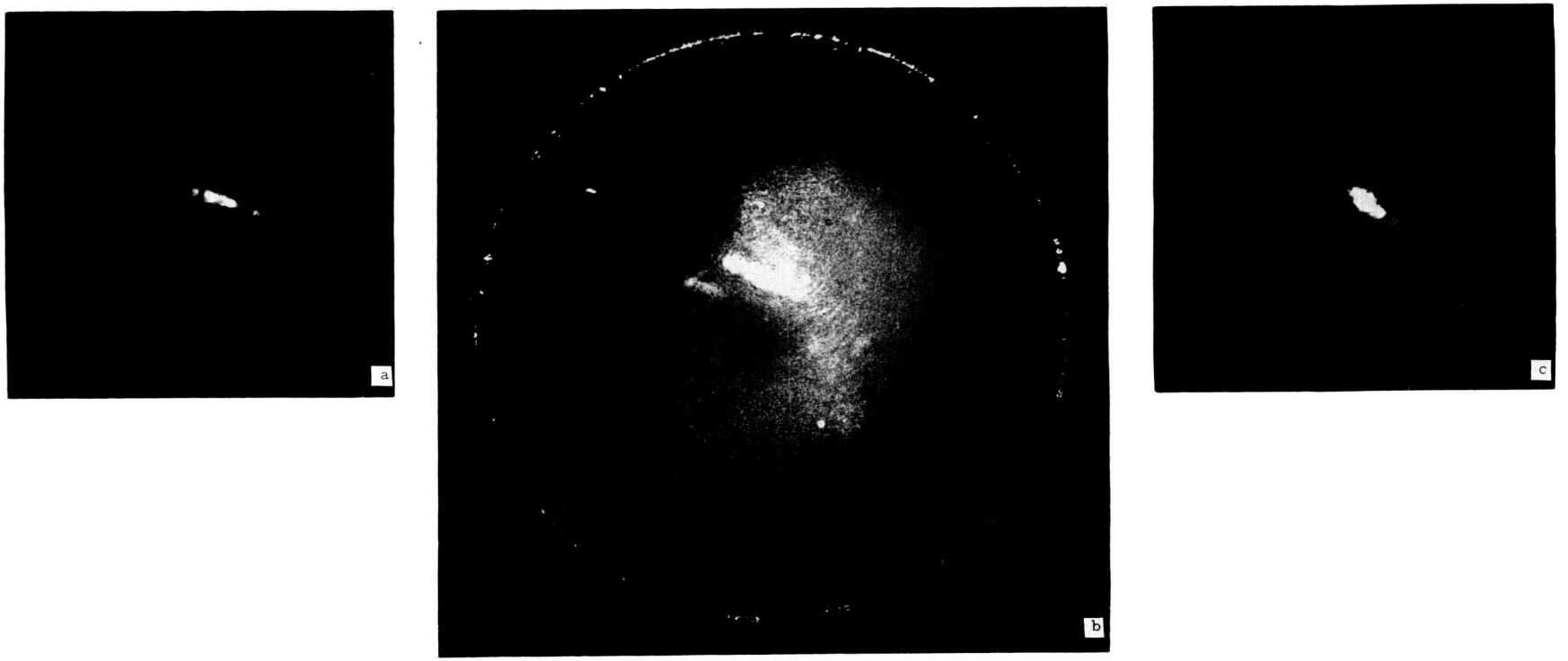

Fig. 18--Near-field patterns of a $CaWO_4$:Nd laser operated at (a) pumping energy of 7.9 J; (b) pumping energy of 6.2 J; and (c) pumping energy of 7.9 J after irradiation with γ rays. Total dose, 4,000 rads

The reason for its appearance is not completely understood. Figure 18(c) shows the emission of the laser after it had received a 4,000-rad dose of γ rays. Taken at a pump level of 7.9 J, it shows little change from (a) except perhaps for a slight enlargement of the filaments. Figure 19 shows the effects of proton irradiation on the near-field pattern of a $CaWO_4$:Nd laser rod.

3.5 Far-Field Patterns

The intensity distribution of the emission pattern at a large distance from the laser is referred to as the far-field or Fraunhofer pattern. For the ideal case where the output of the laser is diffraction limited, the far-field pattern is given by the Fraunhofer pattern of the Airy disc of diameter d where $d = (1.22\,\lambda)/\theta$ where θ is the divergence angle.

The far-field pattern is of special interest in communications where a small beam spread or divergence is desired for maximum signal strength. To measure the far-field pattern, some workers[35] use a lens focussed at infinity. We have found it more convenient to eliminate the lens and observe the pattern directly. The arrangement used is shown in Figure 20, and uses the same camera body as before. The shutter is used to exclude stray light when the laser is not emitting. Typical far-field patterns are shown in Figures 21 through 25.

3.6 Optical Quality of Laser Rods Studied by Far-Field Pattern of Transmitted Gas-Laser Beam

The optical quality of a laser rod can be studied in a passive manner by passing a coherent beam of light from a He-Ne laser through the crystal, where it is distorted by the inhomogeneities in the crystal. The resulting pattern is recorded as a Fraunhofer pattern by the camera. The method is quite sensitive and simple, and provides an accurate representation of the effect of the distortions on a coherent beam of light. The arrangment used is shown in Figure 25. Figures 21, 22, and 23 compare the transmitted beam characteristics of several laser rods to the far-field patterns actually observed when the crystals are lasing. It can be seen that crystal perfection is a major factor in the symmetry obtained in the laser beam. Figure 24 shows three far-field patterns of a YAG:Nd laser: (a) is due to the beam of a gas laser; (b) is the far field at a pump energy of 30.2 J; (c) is the pattern after heavy irradiation with protons and at a pump energy of 46.8 J, which corresponds approximately to the same output power as (b).

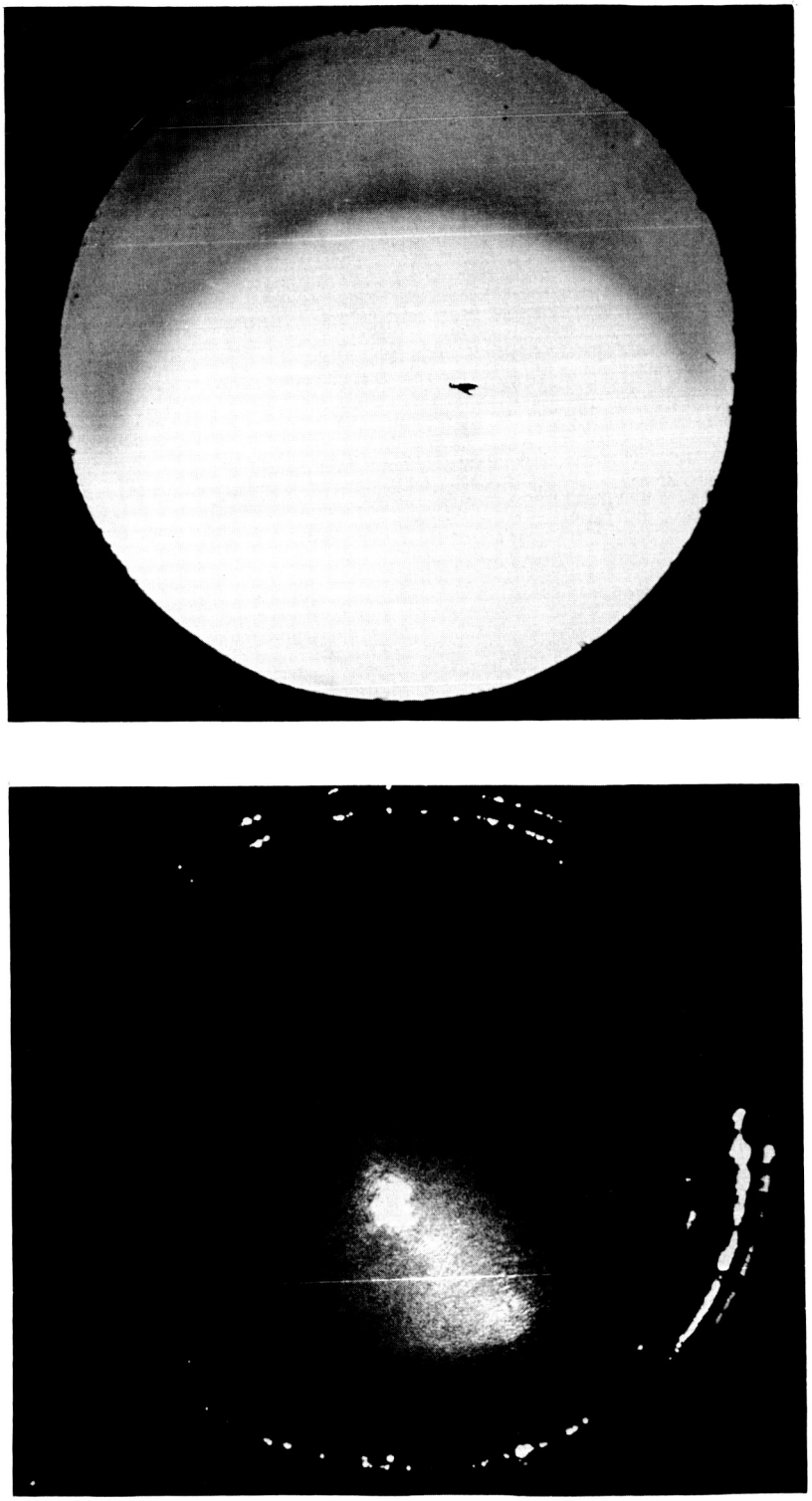

Fig. 19--(a) Proton-induced coloration in a $CaWO_4$:Nd laser rod;
(b) Laser near-field, showing absence of lasing or super-radiance in irradiated area

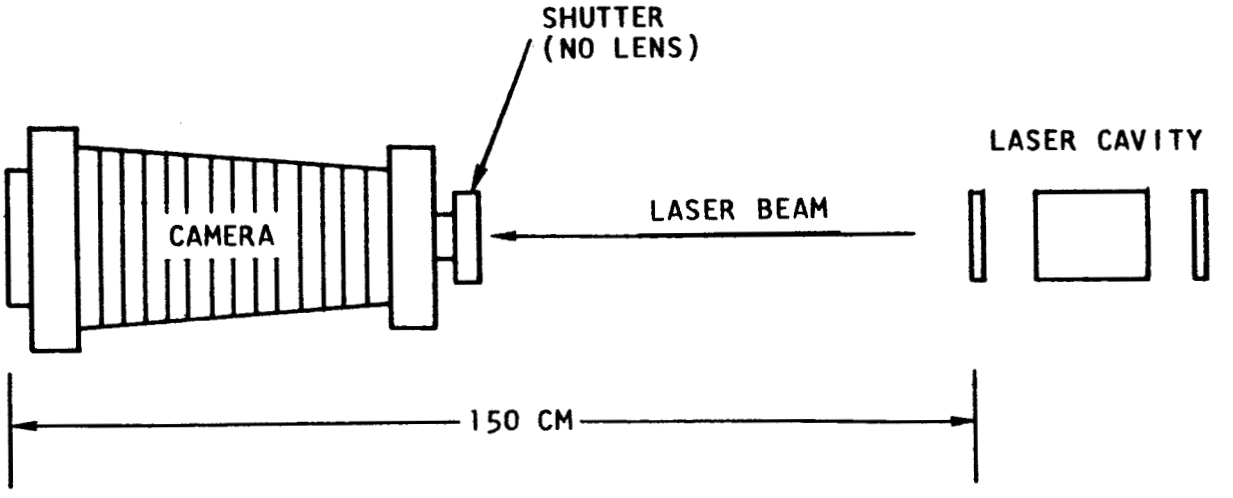

Fig. 20--Experimental arrangement used to photograph far-field patterns

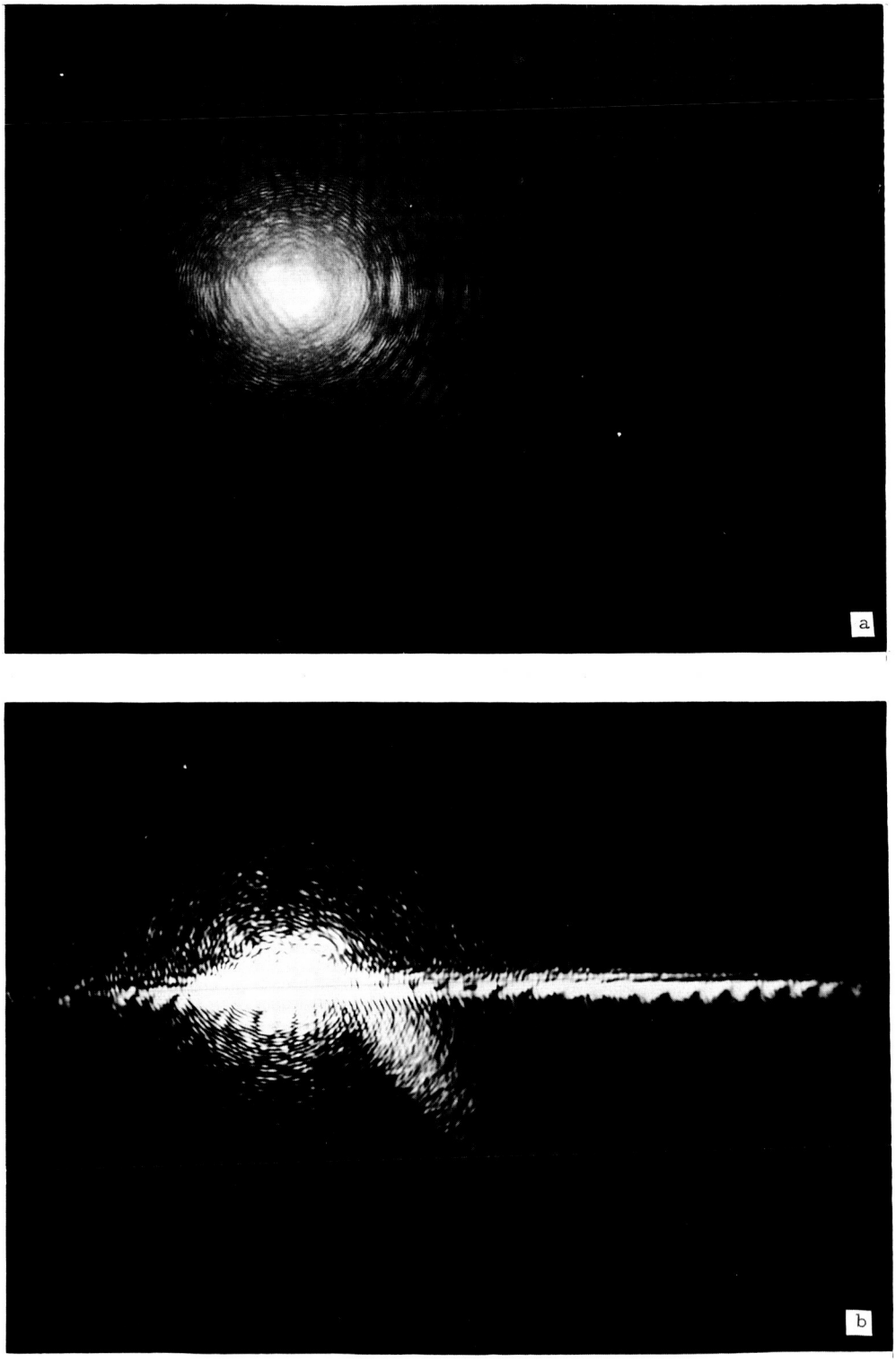

Fig. 21--(a) Far-field pattern of a $CaWO_4$:Nd laser rod; pump energy, 15 J; (b) transmitted beam of a gas laser, distorted by the laser rod. Note similarity to far-field pattern

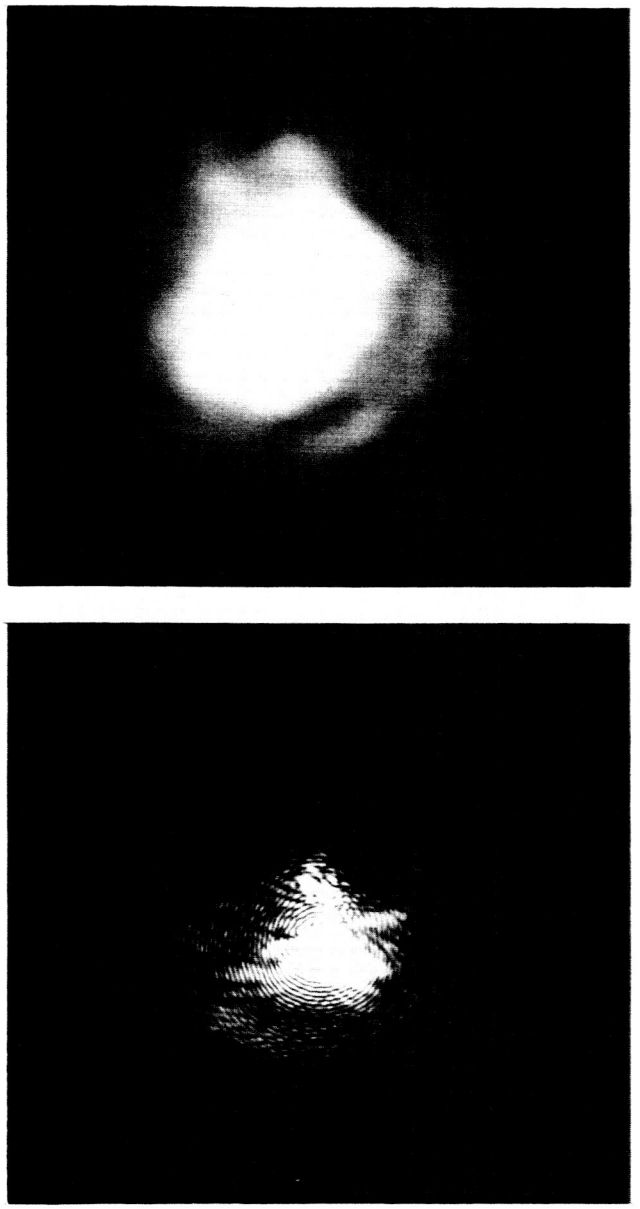

Fig. 22--$CaWO_4$:Nd. (a) Far-field pattern of laser rod--pump energy, 17.5 J; (b) far-field pattern of transmitted gas laser beam

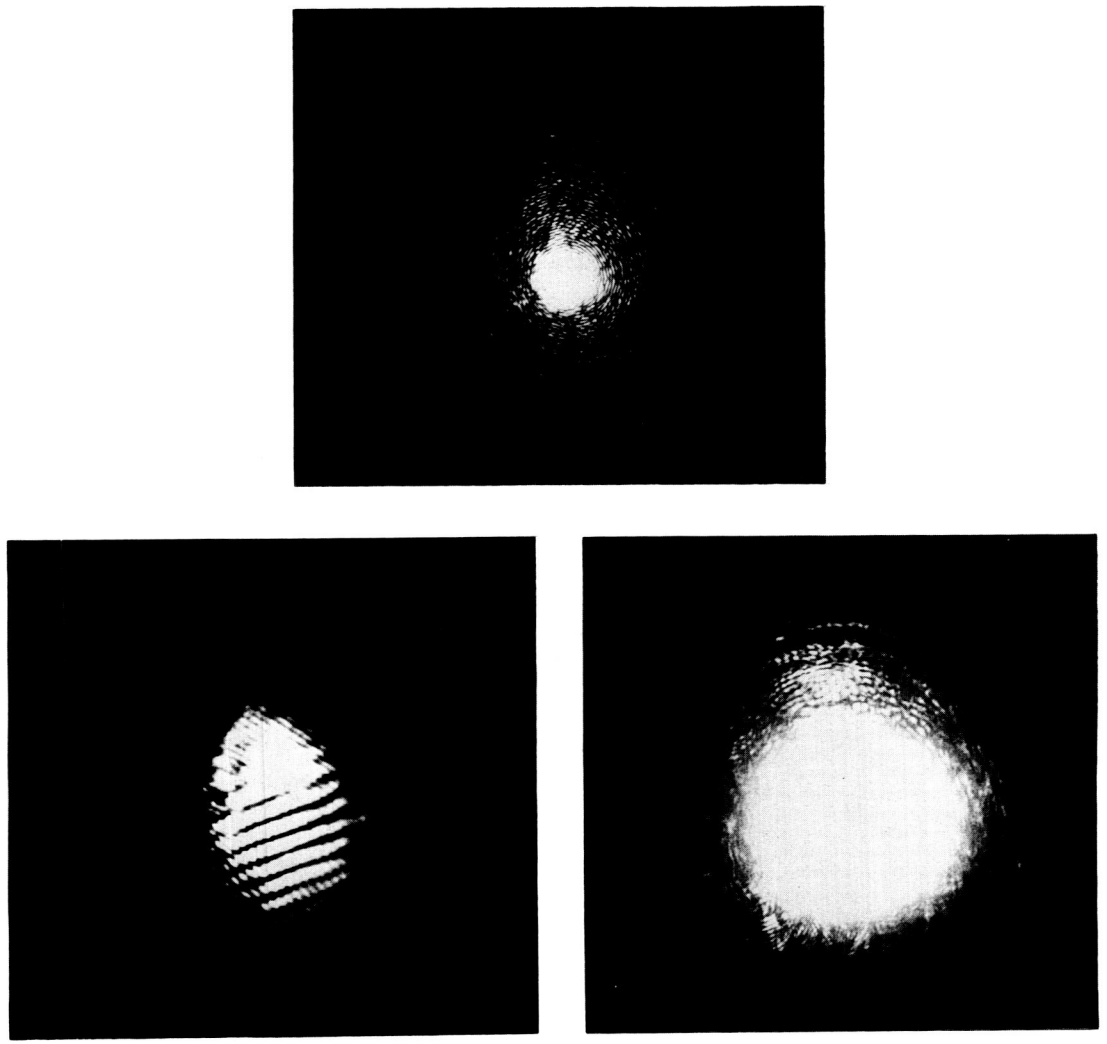

Fig. 23--Glass:Nd. (a) Far-field pattern of a transmitted gas laser beam showing good optical properties; (b) far-field pattern at slightly above threshold, 287 J; (c) far-field pattern at high pump power, 409 J

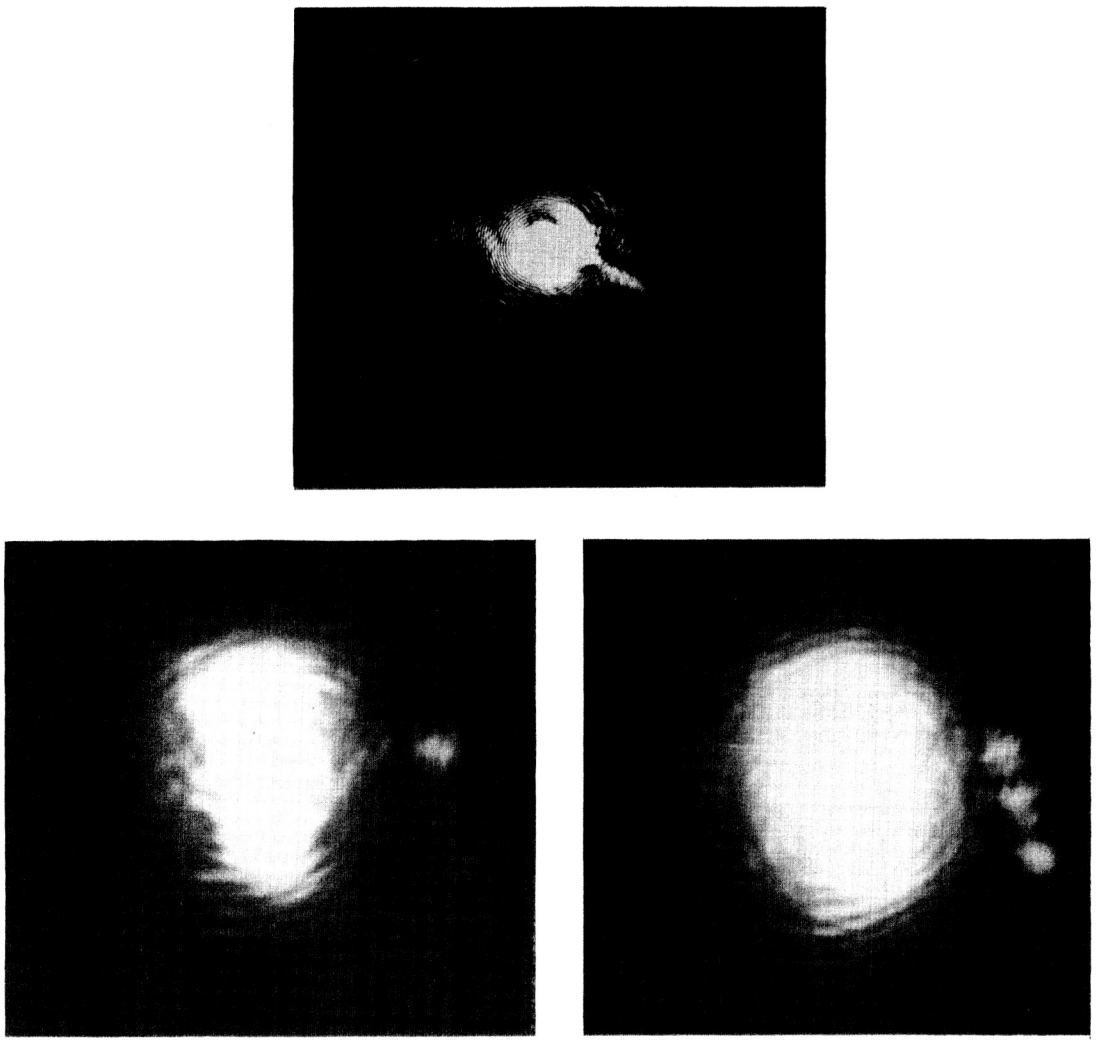

Fig. 24--YAG:Nd. (a) Far-field of a transmitted gas laser beam; (b) far-field pattern before irradiation, 30.2 J; (c) far-field pattern after irradiation with protons, 46.8 J

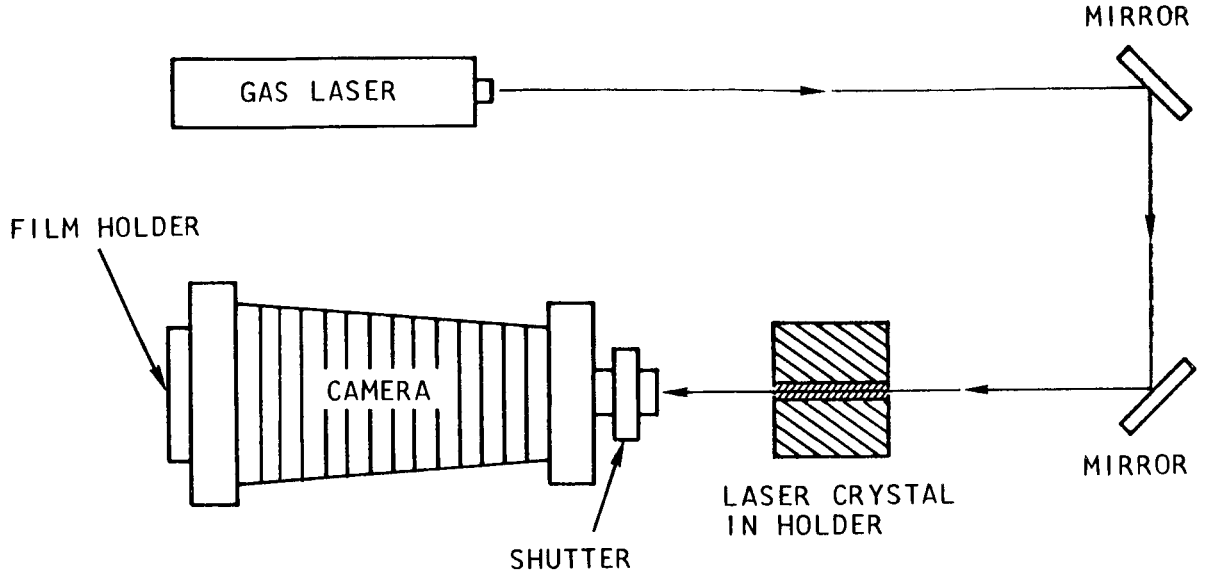

Fig. 25--Experimental arrangement used to study optical perfection

3.7 Light Scattering

Scattering of light through small angles is an important source of optical loss in laser rods and can be studied in principle by measuring the loss through scattering of a gas laser beam passing through the rod. This was attempted for the laser rods studied in this program, but the rods were of poor optical quality (as seen by the far-field results in Section 3.6) and no useful results could be obtained, since no change could be observed on irradiation.

3.8 Interferometry

Another method of studying optical quality is to use an interferometer, typically a Twyman-Green. To see if any change in index of refraction could be measured upon irradiation, rods were irradiated with a dose of 32-Mev protons ($\sim 10^{13}$ cm^{-2}) sufficient to cause marked browning. The rods were of thickness such that the protons penetrated only part-way. Figure 26 gives photographs of the rods, showing the typical sharp cutoff of the range for protons. Interference patterns were determined for these rods before and after irradiation, and should provide an unusually sensitive test for any change in optical path length, since only a portion of the rod has been affected. However, no change in patterns could be seen. It thus appears that this method is not sensitive enough to be useful.

3.9 Optical Absorption

Optical absorption forms a useful "passive" test for the effects of irradiation on optically pumped lasers, since it shows the formation of color centers which appear to be an important source of optical loss.

Special holders were constructed to allow laser rods to be inserted into the measurement compartment of a Cary Model-14 spectrophotometer and a Beckmann DB spectrometer. In each case, problems arise because the sample is thick and changes the focus of the optical system of the spectrophotometer in a manner that depends on wavelength, thus changing the 100%-transmission value. However, this can be corrected for by running a sample before and after irradiation, or by using two similar samples, inserting one into the reference beam.

3.10 Apparatus to Run in TRIGA Reactor

The TRIGA reactor core is under some 15 ft of water used as partial moderator and shielding. Our original apparatus to expose lasers to radiation from the reactor brought the laser light out through a long tube to the surface of the water where it was monitored by a phototube. It was found that this system did not give reproducible results because of slight

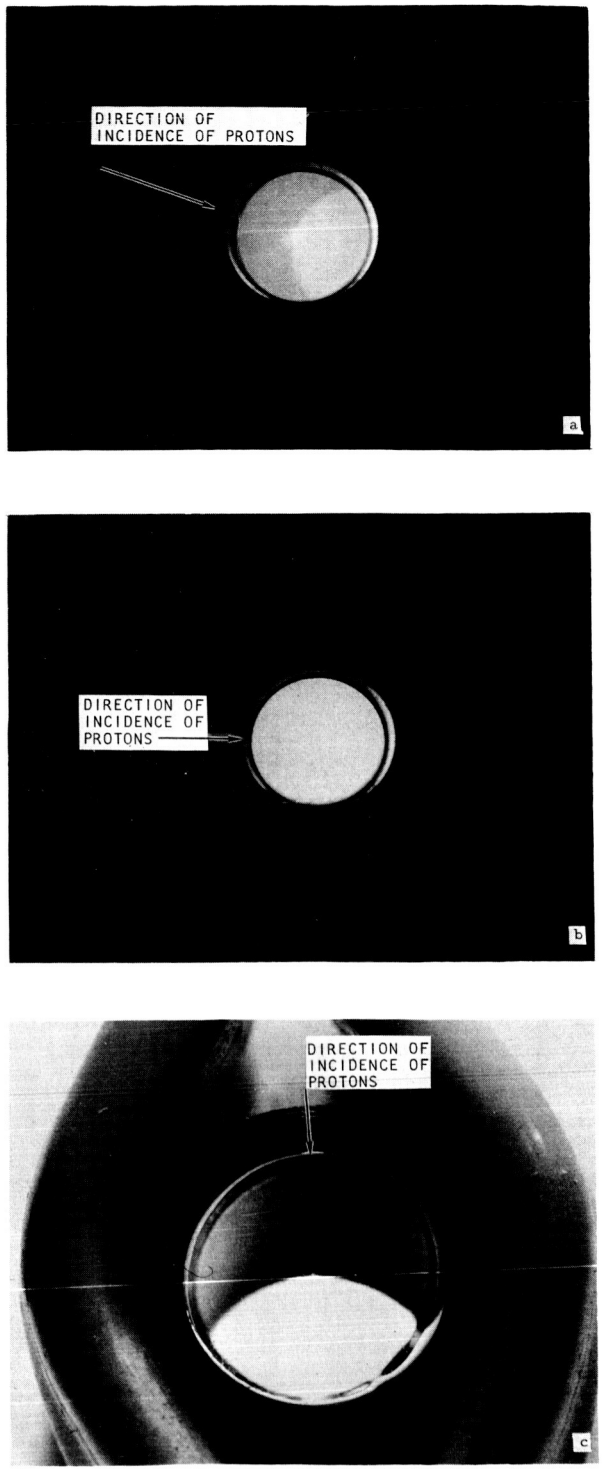

Fig. 26--Coloration produced by protons in (a) $CaWO_4$, (b) Al_2O_3, (c) borosilicate glass

displacements of the tube. Accordingly, a new apparatus was built which incorporated the phototube in the same watertight housing. It is shown in a photograph in Figure 27 and in diagram form in Figure 28.

The apparatus used to monitor the radiation incurred by the laser system consists of a special ionization chamber, mounted next to the laser, and circuitry used to measure the current through the chamber. A low voltage, typically 90 V to minimize leakage, is applied to the chamber, using a circuit similar to that shown schematically in Figure 29. The chamber operated at this voltage is linear from 1 R/hr to over 10^5 R/hr. The dose rate is determined by measuring the current flowing, and multiplying by the chamber constant; and the total dose is found by integration of the microammeter output or of the strip-chart record.

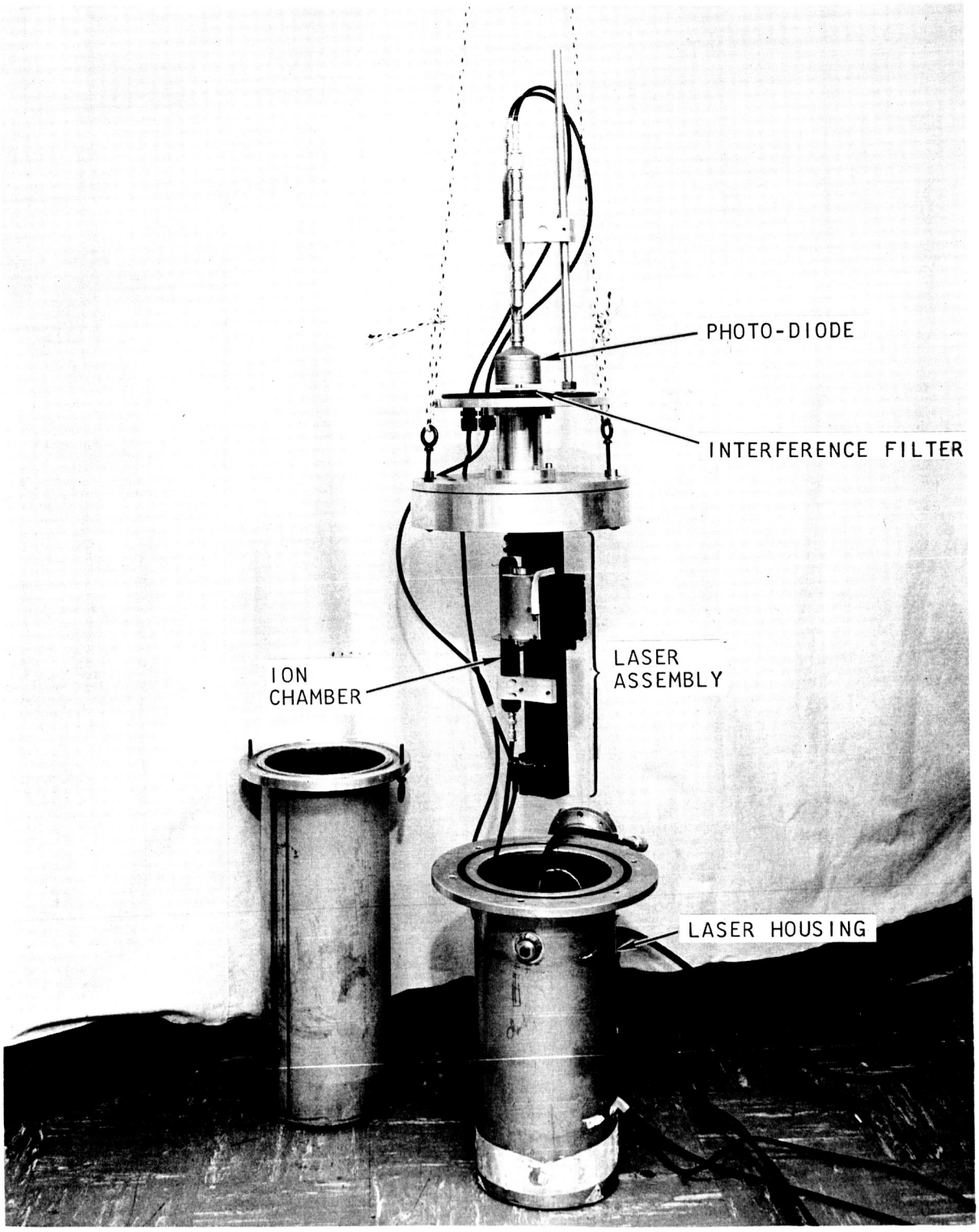

Fig. 27--Water-tight cell used to measure laser output during gamma irradiation in TRIGA reactor

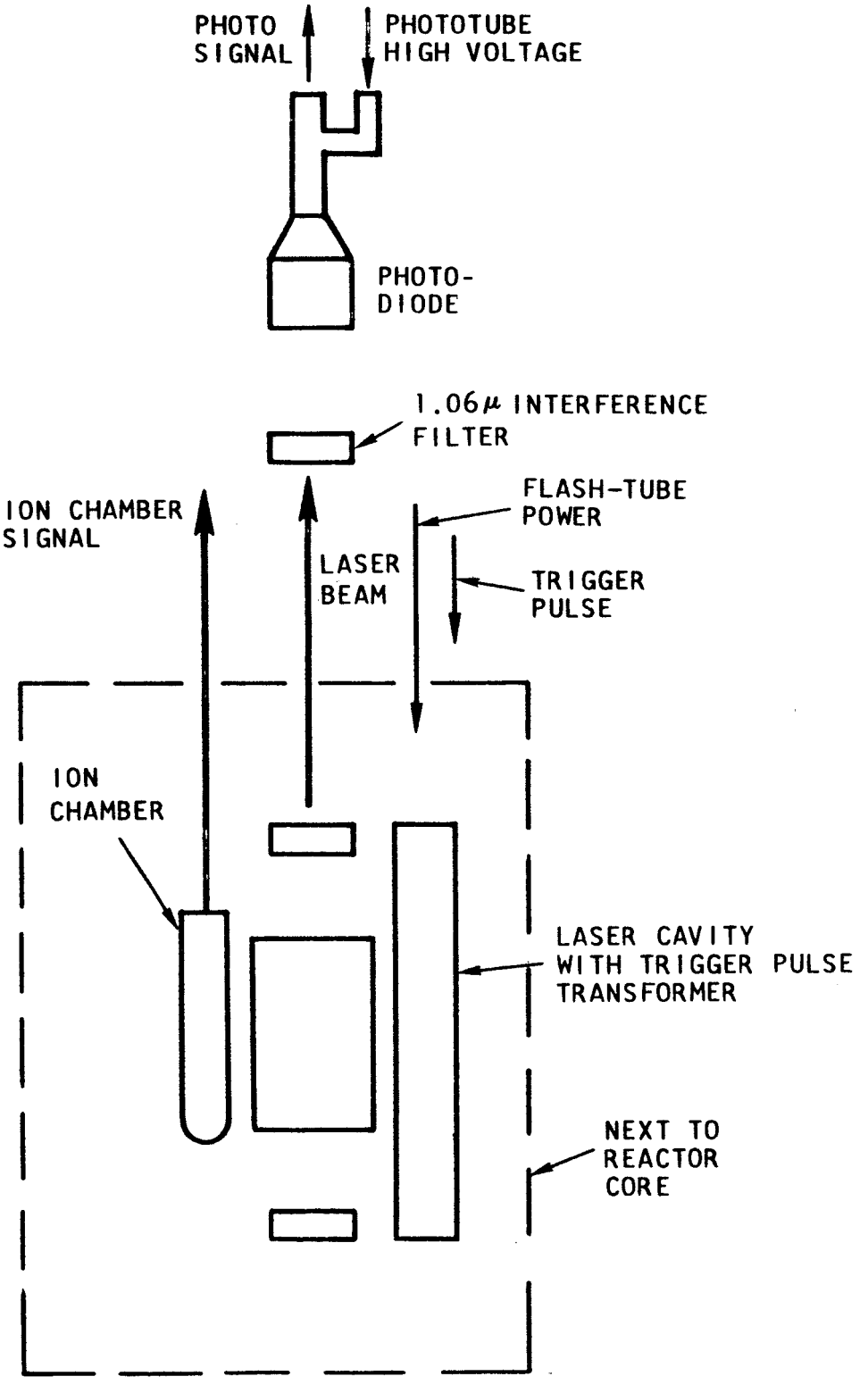

Fig. 28--Schematic showing internal arrangement of cell in Figure 27

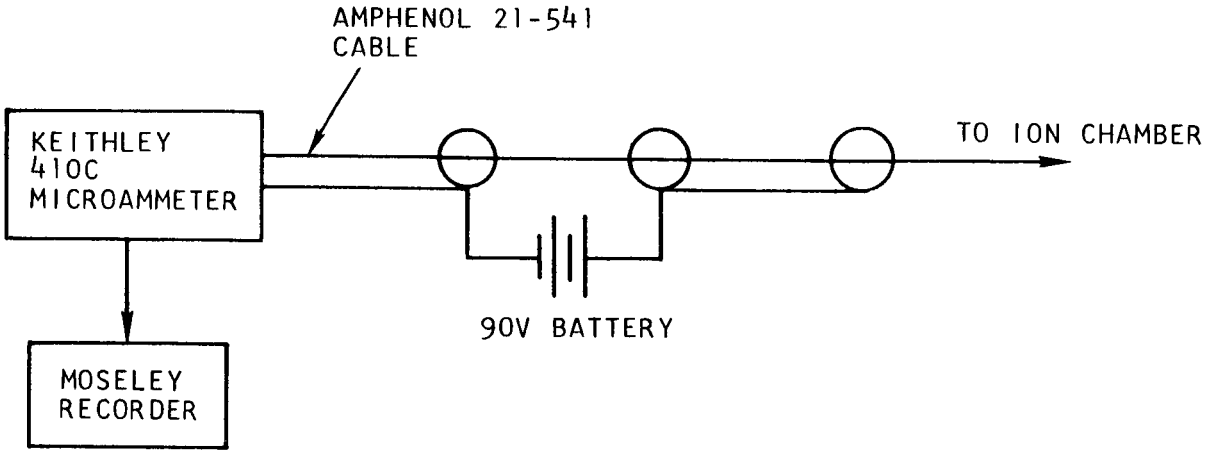

Fig. 29--Circuitry used to measure ion chamber current

IV

RESULTS

The work reported here has been chiefly aimed at exploring the phenomenology of the effects of irradiation on lasers; the acquisition of final data, based on decisions as to what types of data are reliable, meaningful, and useful was deferred until the next portion of this program.

4.1 Output-input Curves on Optically Pumped Lasers

Using the equipment described in Section III, it was possible to measure output versus input curves for optically pumped lasers such as $CaWO_4$:Nd, YAG:Nd, and glass:Nd, although some difficulties were encountered with a high-threshold ruby rod.

For the low-threshold laser rods, the output-input curves were linear, showing moderately low scatter and a sharp threshold. An example is given in Figure 30.

At higher pumping energies obtained by switching in larger values of capacitors, some difficulties were encountered. Differences in output energy were obtained, with nominally identical input energies, from different values of capacitors. The system behaved as if some of the capacitors had an effective value different from the value measured with a low-frequency bridge. This effect could be corrected by simple "scaling": assigning an arbitrary value to each of the capacitors to make the measured output-input curves match. It could also be avoided by using only one high-valued capacitor and inserting absorbing filters between the flash lamp and laser rod to obtain points for low input energies. A more serious problem was that at very high input energies, required to pump ruby, or Nd lasers after heavy irradiation, the output-input plots showed very severe scatter. This is thought to be due to variations in the amount of discharge given by the high-value capacitors, which are now being replaced by another type.

With the external-mirror cavity, it often proved to be difficult to repeat measurements when the laser rod was removed and replaced. The mirrors of the cavity are aligned with an auto-collimator, which can also be used to check that the end of the laser rod is parallel to the mirrors. It is also necessary to rotate the laser rod about its axis to maximize its output; presumably this is because the ends of the laser rod are not exactly parallel. With these precautions, reproducible results can generally be obtained, but it is now planned to make the final measurements comparing the effects of

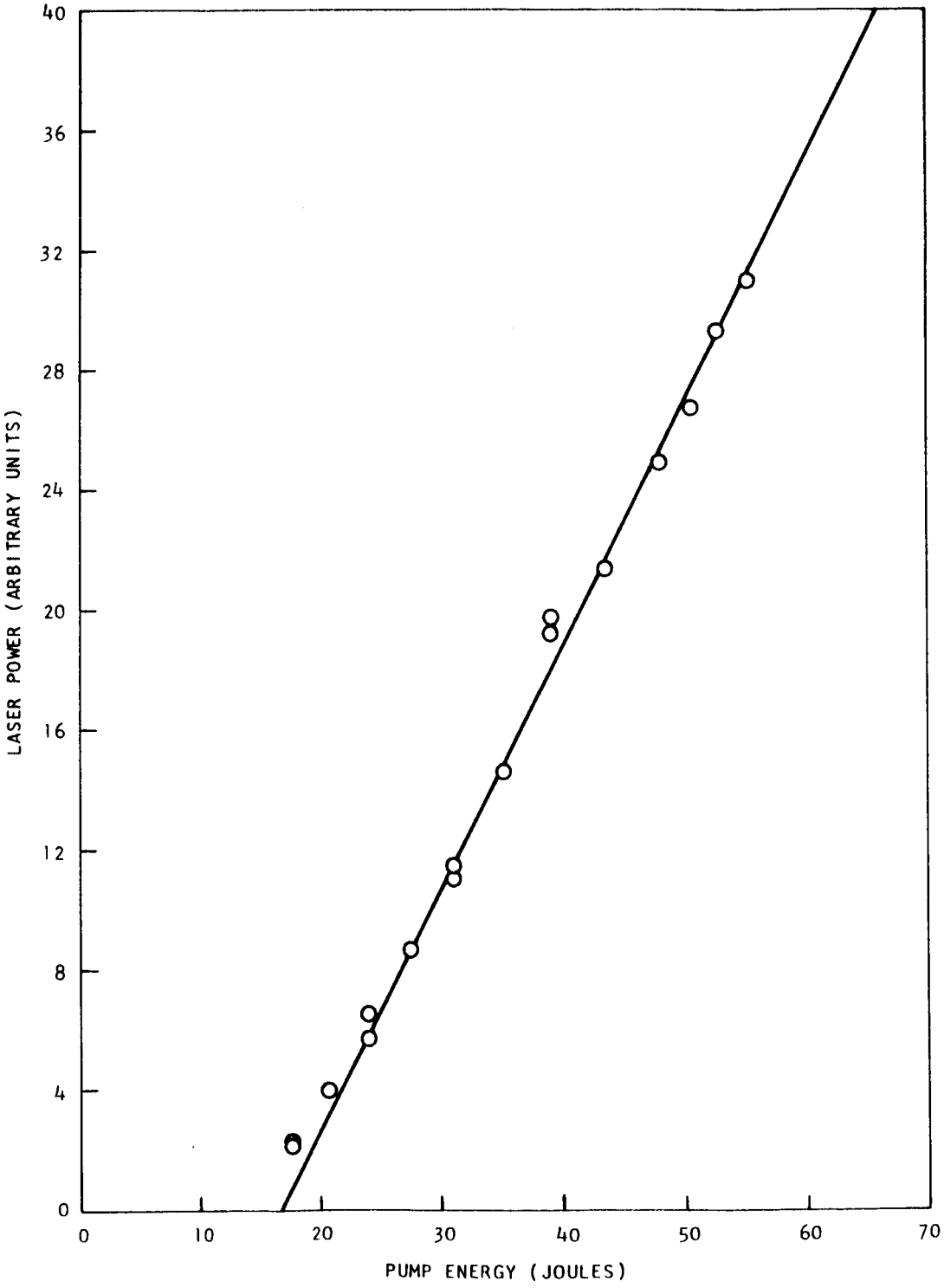

Fig. 30--Power output versus energy input for $CaWO_4$:Nd laser rod before irradiation

absolutely known doses of various types of radiation, using lasers with mirrors directly evaporated on the ends, as these are expected to give more reproducible results.

The theory of the power output of a four-level laser has been treated by Yariv.[36] This predicts that the measured stimulated emission will be zero up to a threshold input power, and will then increase linearly with input, as observed in Figure 30. The treatment can be extended to include effects of optical losses due to irradiation. Optical losses are believed (see below) to be the major mode by which irradiation affects lasers. Yariv accounts for the loss of photon energy in the optical resonator by using a photon lifetime t_{photon}. He divides the losses into two main categories: (a) Losses due to attenuation, scattering and diffraction within the resonator, and the losses due to absorption in the reflectors. These are referred to as cavity losses. (b) Losses due to the finite transmission of the end reflectors, i.e., to the power delivered externally. He then writes

$$\frac{1}{t_{photon}} = \frac{1}{t_R} + \frac{1}{t_x} \quad ,$$

where t_R accounts for the losses in (a), while t_x represents those in (b).

To these, we add a further loss, due to irradiation, which we represent by an equivalent lifetime t_I, and we define t_o to correspond to the losses before irradiation, so that

$$\frac{1}{t_o} = \frac{1}{t_R} + \frac{1}{t_x} \quad .$$

If we assume that all the effects of irradiation can be lumped into a single term t_I, we may modify his equations (10) and (11) to include a photon lifetime given by

$$\frac{1}{t_{photon}} = \frac{1}{t_R} + \frac{1}{t_x} + \frac{1}{t_I} \quad .$$

This equation may be written as

$$P_s = P_{fc}\left(\frac{R_2' t_{photon}}{p} - 1\right)$$

where

P_s = stimulated emission power,

P_{fc} = fluorescent power at threshold,

R_2' = effective rate of pumping into the upper laser level,

p = number of modes "in contact with the laser transition."

(For a discussion of these quantities, see the original article by Yariv[36]).

Modifying to include t_I,

$$P_{fc}' = \frac{p\,h\nu}{t_{photon}} = \frac{p\,h\nu}{t_o}\left(1 + \frac{t_o}{t_I}\right)$$

$$= P_{fc}^{\,o}\left(1 + \frac{t_o}{t_I}\right)$$

where P_{fc}' and $P_{fc}^{\,o}$ refer to after and before irradiation, and

$$\frac{R_2'\,t_{photon}}{p} = \frac{R_2'}{p}\,\frac{t_o\,t_I}{t_o + t_I} = \frac{R_2'}{p}\,\frac{t_o}{1 + t_o/t_I} \quad .$$

We note that P_{ex}, the externally measured stimulated emission power, is given by

$$P_{ex} = P_s\left(1/t_x \Big/ 1/t_{photon}\right) = P_s\,\frac{t_o}{t_x}\,\frac{1}{1 + t_o/t_I} \quad ,$$

so that

$$P_{ex} = P_{fc}^{\,o}\,\frac{t_o}{t_x}\left[\left(\frac{R_2'}{p}\,\frac{t_o}{1 + t_o/t_I}\right)\right] - 1 \quad .$$

Now R_2' is assumed proportional to input pump lamp power (and thus to the energy, if the shape of the lamp emission versus time curve is constant), so that we may write

$$\frac{R_2' t_o}{p} \quad \text{is proportional to pump power,}$$

or, for convenient scaling,

$$= \frac{P_{pump}}{P^o_{threshold}}$$

where $P^o_{threshold}$ is the pump power at threshold before irradiation. We may then write

$$P_{ex} = P^o_{fc} \frac{t_o}{t_x} \left[\frac{P_{pump}}{P^o_{threshold} \left(1 + t_o/t_I \right)} - 1 \right] .$$

The threshold pump power after irradiation is then given by

$$P'_{threshold} = P^o_{threshold} \left(1 + \frac{t_o}{t_I} \right) ,$$

while the slope S is given by

$$S = \frac{\Delta P_{ex}}{\Delta P_{pump}} = \frac{P^o_{fc} (t_o/t_x)}{P^o_{threshold} \left(1 + t_o/t_I \right)} ,$$

so that the ratio of the slope S' after irradiation to S_o, the slope before irradiation, is given by

$$S'/S_o = \left(1 + \frac{t_o}{t_I} \right)^{-1} .$$

Accordingly, on this model, irradiation would be expected to increase the threshold pump power by a factor $1 + (t_o/t_I)$ and decrease the slope of the output power versus input power line by the same factor.

In many cases, this behavior was found. An example is given in Figure 31. Here the threshold of a YAG:Nd rod was increased from 15.2 to 17.5 J by a ratio of 1:1.15. The slope was decreased by a factor of 53.5/46.8 = 1.14.

The value obtained for $1 + (t_o/t_I) = 1.15$ corresponds to $t_I = 0.15\ t_o$, one-sixth of the losses already present. The mirror losses were 6% per pass; assuming that these were the main original sources of loss, then the additional loss introduced by the irradiation was ~1% per pass.

The good agreement between shift in threshold and change of slope suggests the use of the parameter t_I as a measure of the effects of irradiation upon optically pumped lasers. However, this parameter slope does not always prove to be sufficient. An example is given in Figure 32, for 32-MeV proton irradiation of YAG:Nd. Here the curve on the left represents the initial output-input curve, and that on the right, the curve taken 5 min after irradiation. The ratio of the thresholds is 1.46 and of the slopes 1.44, indicating good agreement with the above simple theory. However, the intermediate curve, taken 150 min after irradiation, shows apparent spontaneous room-temperature annealing of the threshold, but not of the slope. The behavior may be due to measurement error (e.g., mispositioning of the laser rod in the cavity) or to a real effect associated with the proton irradiation, e.g., a change in line width which would change the number of modes.

Further, a good agreement between change of slope and change of threshold does not indicate that the optical-loss model given above is correct, because it is not unique in making that prediction. For example, if irradiation reduced the efficiency of pumping for a laser by introducing color centers that could compete with the doping ions for the pump light, the effect would correspond to changing the scale on the pumping energy axis. This would increase the threshold by the factor associated with the reduction in efficiency and reduce the slope of the output-input curve by the same factor. This effect is, however, only likely to be important at high radiation doses, where the crystal is highly colored. A 1% increase in absorption per lengthwise pass of a laser rod would produce totally negligible absorption in the thickness direction to compete in absorbing pump light.

The effects on threshold and power output can also be shown to be due primarily to optical losses produced by irradiation by using two laser rods in the cavity, which has external mirrors. While one rod is pumped, the other is placed in the light beam inside the cavity, and optical losses in

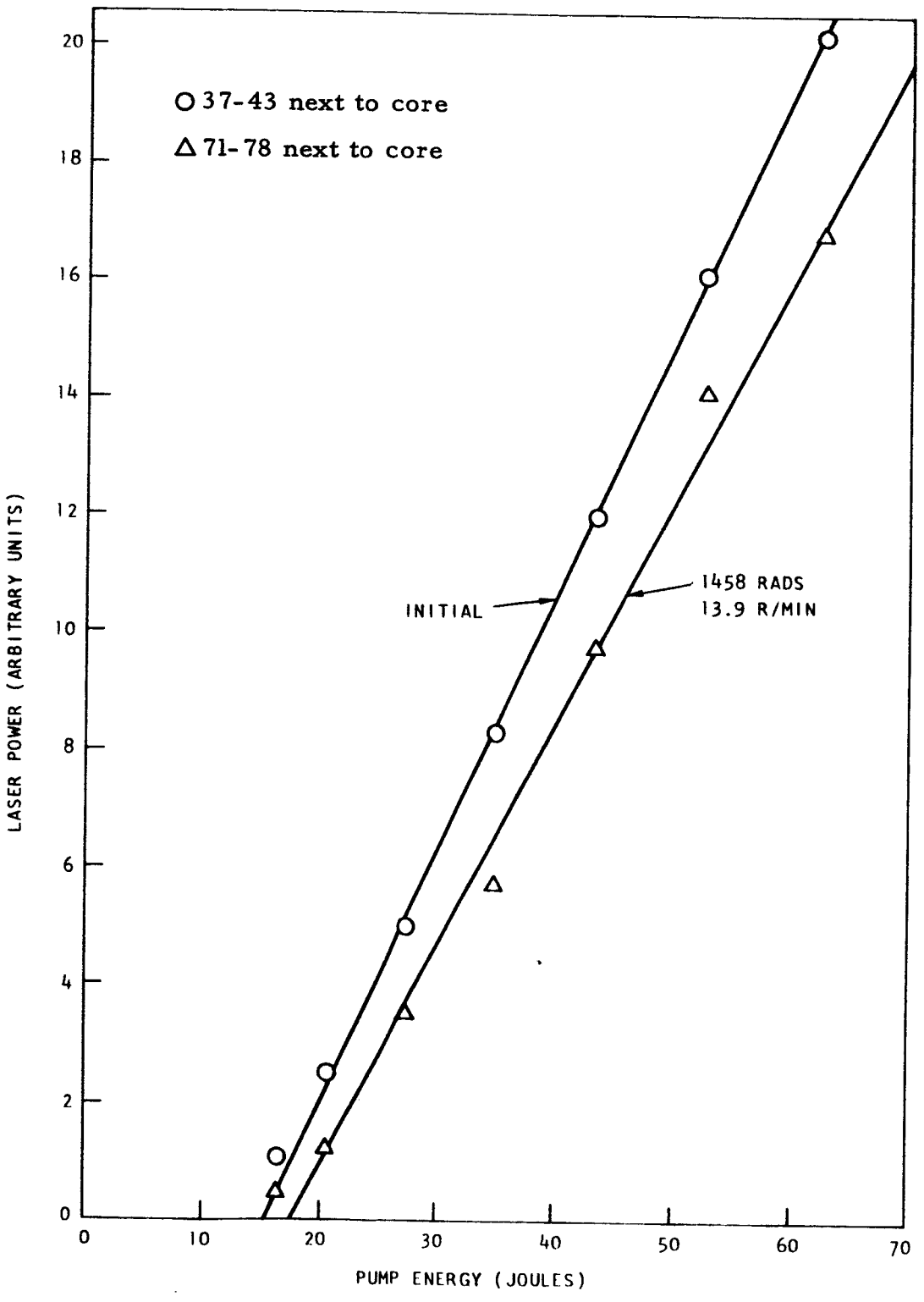

Fig. 31--Power output versus energy input for YAG:Nd before and after irradiation with gamma rays

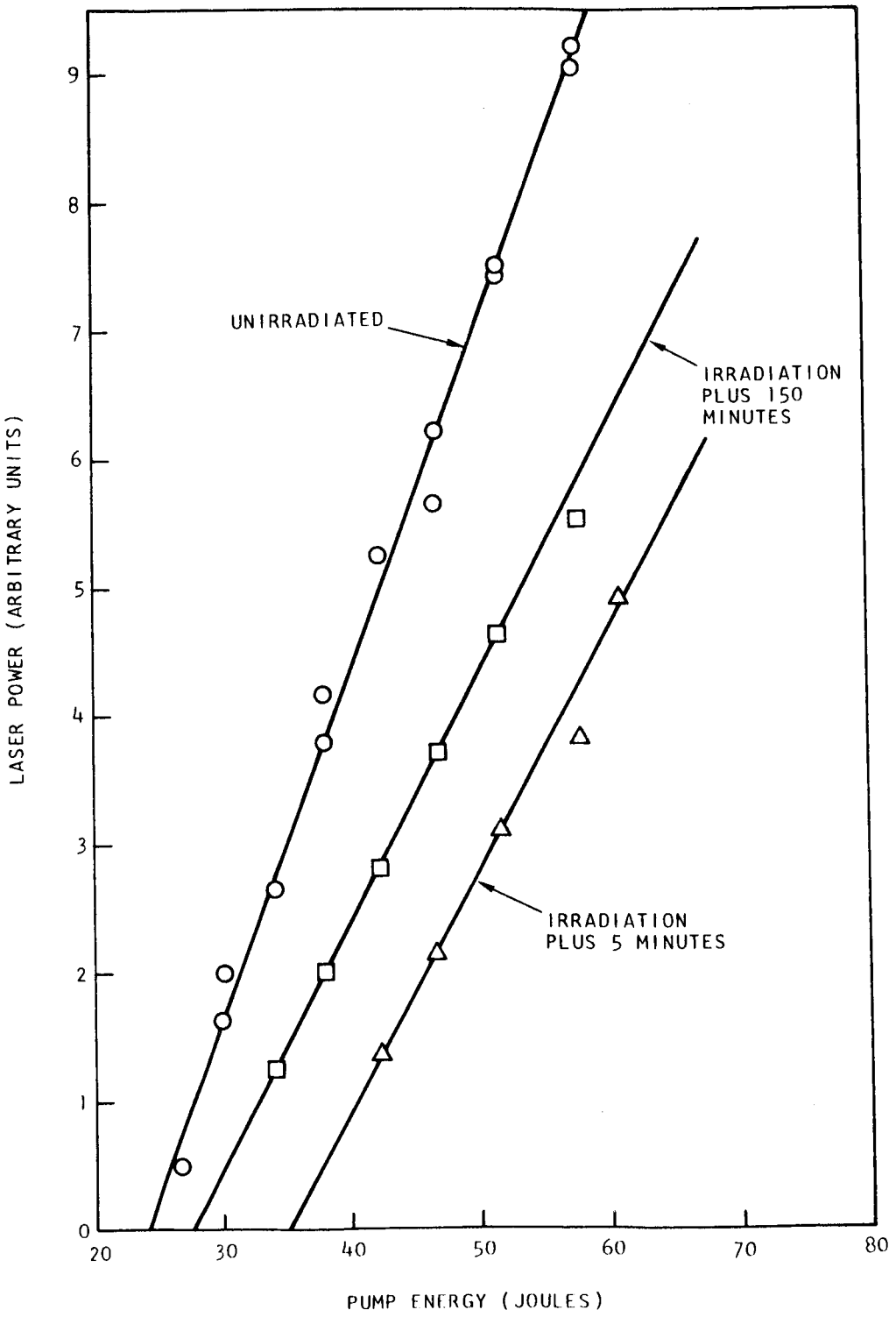

Fig. 32--Power output versus pump energy for YAG:Nd laser before and after irradiation with protons. Degradation shows rapid spontaneous annealing.. Dose: 5×10^9 protons/cm^2

it are "cavity losses" so far as operation of the laser is concerned. With this arrangement, it is found that approximately similar effects on output are produced by irradiating either rod, and the rods may be interchanged with little effect on output. This indicates that the chief effects of irradiation are not due to an interaction between the irradiation and the upper lasing level, i.e., are not due to changes in the pumping efficiency, deexcitation of the upper state, or similar mechanisms. They must, instead, be due to an optical loss mechanism. These experiments are being repeated with rods of higher laser quality.

At the present time, it is felt that interpretation of results in terms of a single parameter t_I is not yet justified. Accordingly, data are usually taken for pumping energies up to 3 to 4 times threshold, so that output-input curves can be plotted. However, a fit to various theories is continuously attempted in order to provide a rational framework for the experimental data and in order to enable eventual optimization of such parameters as mirror reflectivity to be made, for best over-all performance during a mission involving irradiation.

4.2 Optical Bleaching

One of the main interfering effects expected, optical bleaching, was not found to occur with any of the Nd-doped laser rods, at least during any of the several-hundred flashlamp pulses involved in a series of experiments. This means that data can be collected without partial loss of the effects of irradiation each time the laser is fired. However, it also indicates that exposure to light, e.g., sunlight, will probably be ineffective in removing the effects of irradiation in the space enrironment. Further experiments on the effects of long-term low-level illumination on optical bleaching are planned, but it is difficult to avoid confusion with the effects of thermal bleaching which can occur at room temperature (see Sec. 4.4). For ruby, there are marked effects of optical bleaching, but sufficiently definitive studies have not yet been made to unravel the effects.

4.3 Dose-rate Effects and Spontaneous Annealing

The effects of irradiation were found to depend strongly on the rate at which the dose was delivered, as well as the size of the dose and type of radiation. A thorough understanding of this effect is necessary in order to obtain valid measurements, and in order to be able to extrapolate measurements made with (generally) high dose rates in the laboratory to the results expected in the space environment where dose rates are much lower. To study this effect, measurements were made over a wide range of dose rates, using electrons, and γ-rays from the TRIGA reactor and from an isotope source. Dose rates ranged down to a few rads/hr.

Two types of dose rate effects may be distinguished. In one, the effect is due merely to a spontaneous annealing, at the temperature of irradiation and measurement, of the degradation produced by irradiation. An amount of the degradation is lost, depending on the lapse of time between introduction of damage and measurement; if significant loss occurs during the irradiation time, there will be a plainly dose-rate dependent effect. This process can be identified by studying the further recovery that occurs after the end of irradiation. A second type of dose-rate effect occurs when there are two competing processes for damage formation, with different functional dependences on dose-rate, via such intermediate quantities as the instantaneous concentration of electrons and holes produced by the irradiation.

The dose rate effects studied so far can be explained by processes of the first type. A complete understanding would include identification of some measurable parameter that bears a simple relationship to the fundamental damage process, studies of the kinetics of the spontaneous annealing of this parameter (first- or second-order decay), measurements of the growth of this parameter versus dose (not necessarily linear), and comparison of the growth and decay equation with experimental measurements taken during and after irradiations at various dose rates. Although considerable effort has been expended in this direction, the results are not yet satisfactory and show much scatter and many inconsistencies. The chief conclusions are:

a. The parameter t_I is useful for this purpose, but studies are being made to relate t_I to optical absorption in the laser rods (see Sec. 4.5) to see whether the two are equivalent or whether absorption would be better.

b. The introduction of t_I is not proportional to dose, but shows a tendency to saturation.

c. The spontaneous annealing kinetics are not simple; for example, a larger dose or dose rate of irradiation leaves a larger effect that does not spontaneously anneal at room temperature.

d. The effects of electrons and x rays appear to be similar (as expected), but protons give damage harder to anneal.

e. The problem is additionally complicated by purity effects on annealing rates (different rates for different rods of the same material) and by scatter in the data. It is hoped to reduce this last by using rods with mirrors evaporated directly on the ends.

f. For some materials, there appear to be dose rates below which no damage apparently occurs; for example, at <100 rads/hr on YAG:Nd.

Figure 33 shows an example of the output of a laser during continuous low-level irradiation in the TRIGA reactor. It can readily be seen that direct measurements of dose and dose-rate effects are difficult to interpret.

4.4 Annealing

Annealing may occur at the temperature of irradiation and measurement, but can generally be increased by increase of temperature. During this reporting period, some preliminary studies were made of annealing in $CaWO_4$:Nd and YAG:Nd. For CaW_4:Nd irradiated with γ rays or electrons, an anneal of 1/2 hr at 300°C restores the laser action to its original value. There is also considerable room-temperature annealing that seems to vary in extent from rod to rod. Proton irradiation of YAG:Nd produces degradation that also partially recovers at room temperature, as shown in Figure 34. The results of an 8-hr anneal at 100°C are also shown in the same figure, and the change in the input-output curve produced by this anneal are shown in Figure 35. In this material, the effects of electron or γ-ray damage can be removed by an anneal at 100°C, while proton damage cannot be completely removed at this temperature. Annealing is strongly influenced by purity effects. A dramatic example of this was provided by one $CaWO_4$:Nd rod which appeared to the eye to be uniformly colored after removal from a reactor exposure to γ rays. After standing at room temperature for an hour, a narrow filament along the axis of the rod had become perfectly clear, while the rest of the rod was still colored.

4.5 Optical Absorption

Since the effects of radiation on optically pumped lasers seem to occur chiefly via optical losses, measurements were made of optical adsorption produced by irradiation using Beckman DB and Cary Model 14 spectrophotometers and the holders described in Section 3.9. Measurements were made on $CaWO_4$:Nd; it was found that irradiation produces a very broad absorption band, peaking at 4,100 Å and continuing into the infrared. Annealing of this coloration was studied by measuring the absorption after successive half-hour anneals at increasing temperatures. The results are shown in Figure 36. It can be seen that annealing at 200° to 300°C removes the coloration. Annealing at room temperature is shown in Figure 37. A $CaWO_4$:Nd rod was irradiated with γ rays and stored under liquid nitrogen. The optical density at 4,100 Å is shown plotted against the time after removal from liquid nitrogen.

To relate measurements of optical absorption to effects on laser action, it is necessary to measure optical absorption versus wavelength, using the spectrophotometer, and also to measure the very small changes that occur at the laser-emission wavelength: 1.06 μ for Nd-doped lasers. Apparatus for this purpose was assembled during the reporting period and

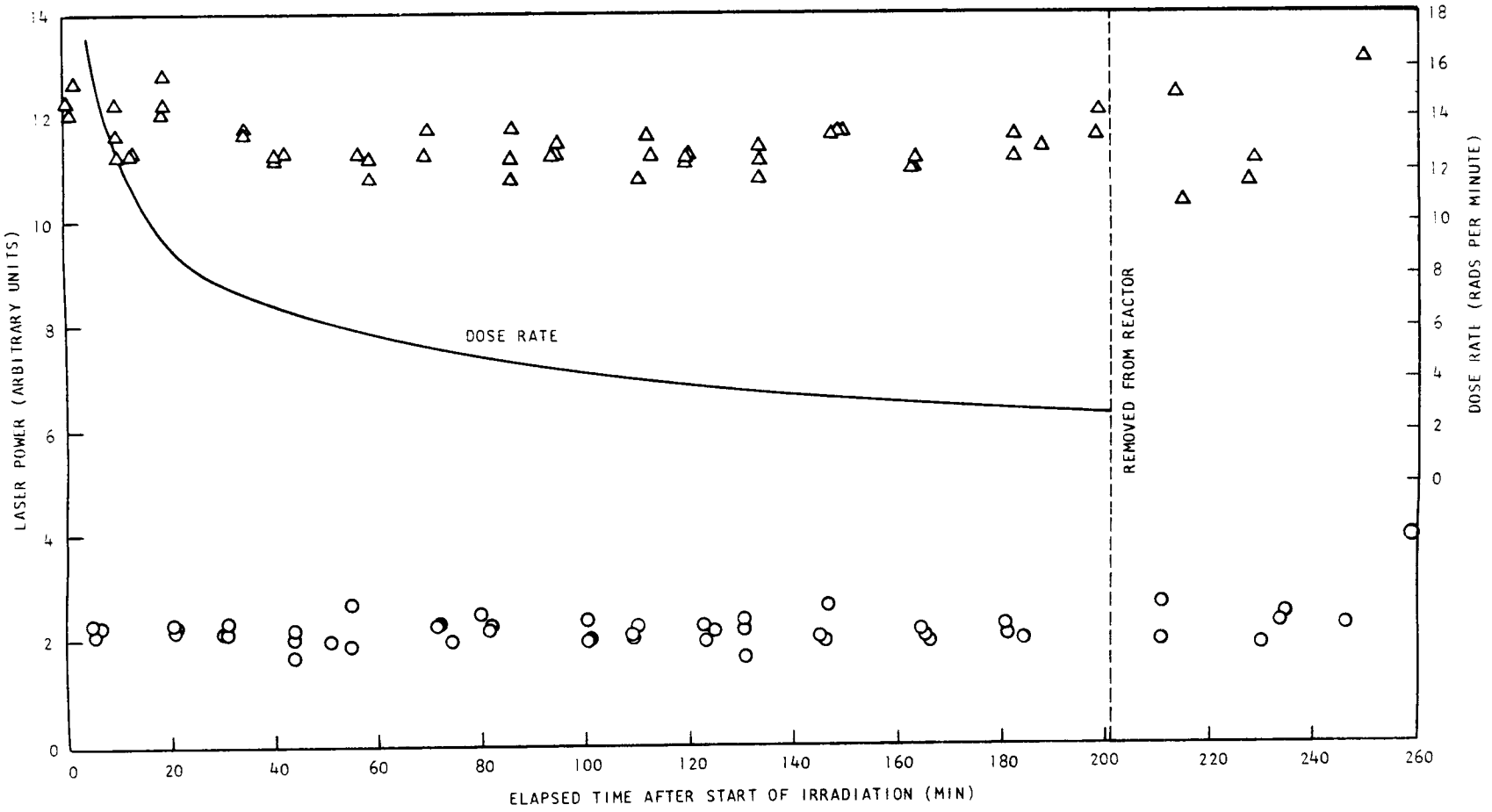

Fig. 33--Power output versus irradiation time for a $CaWO_4$:Nd laser rod at constant pump energy; circles: 17.8 J; triangles: 31.0 J. Gamma dose rate versus irradiation time is shown by solid curve

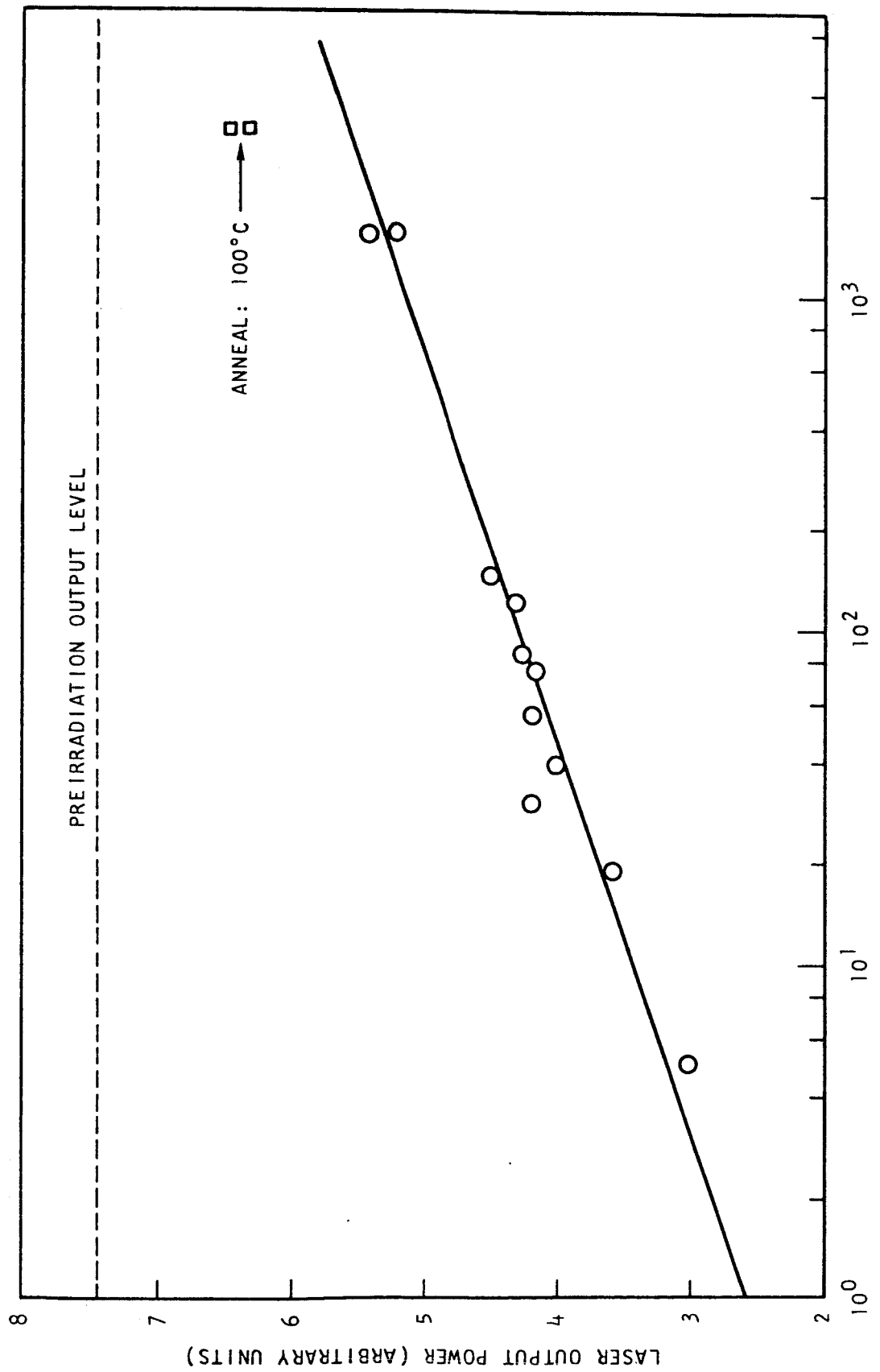

Fig. 34--Recovery at room temperature of laser output from YAG:Nd rod following proton irradiation. Pump-lamp energy constant at 51.6 J. The final points are taken after 8 hr at 100°C

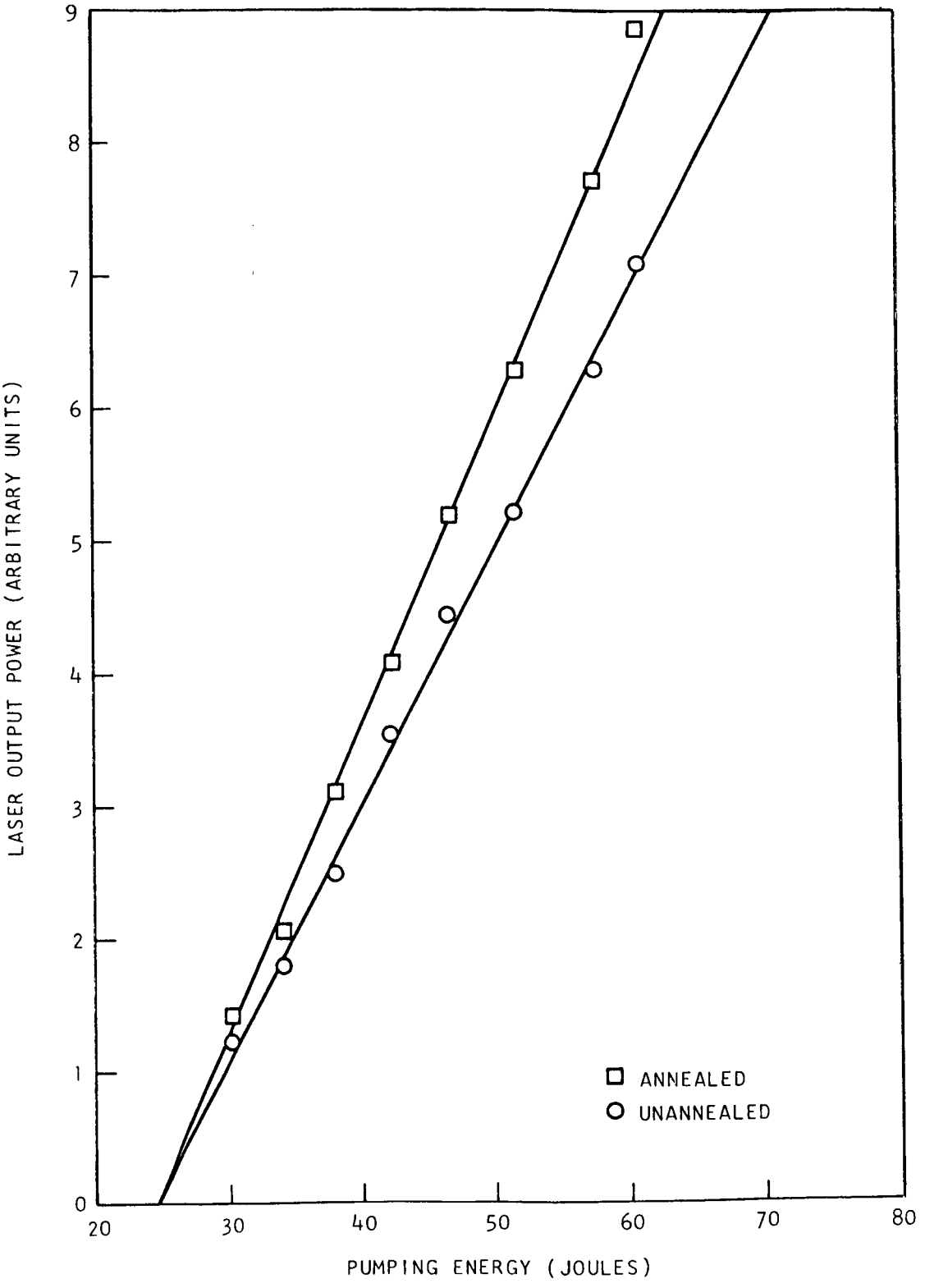

Fig. 35--Output from YAG:Nd laser rod before and after annealing for 8 hr at 100°C

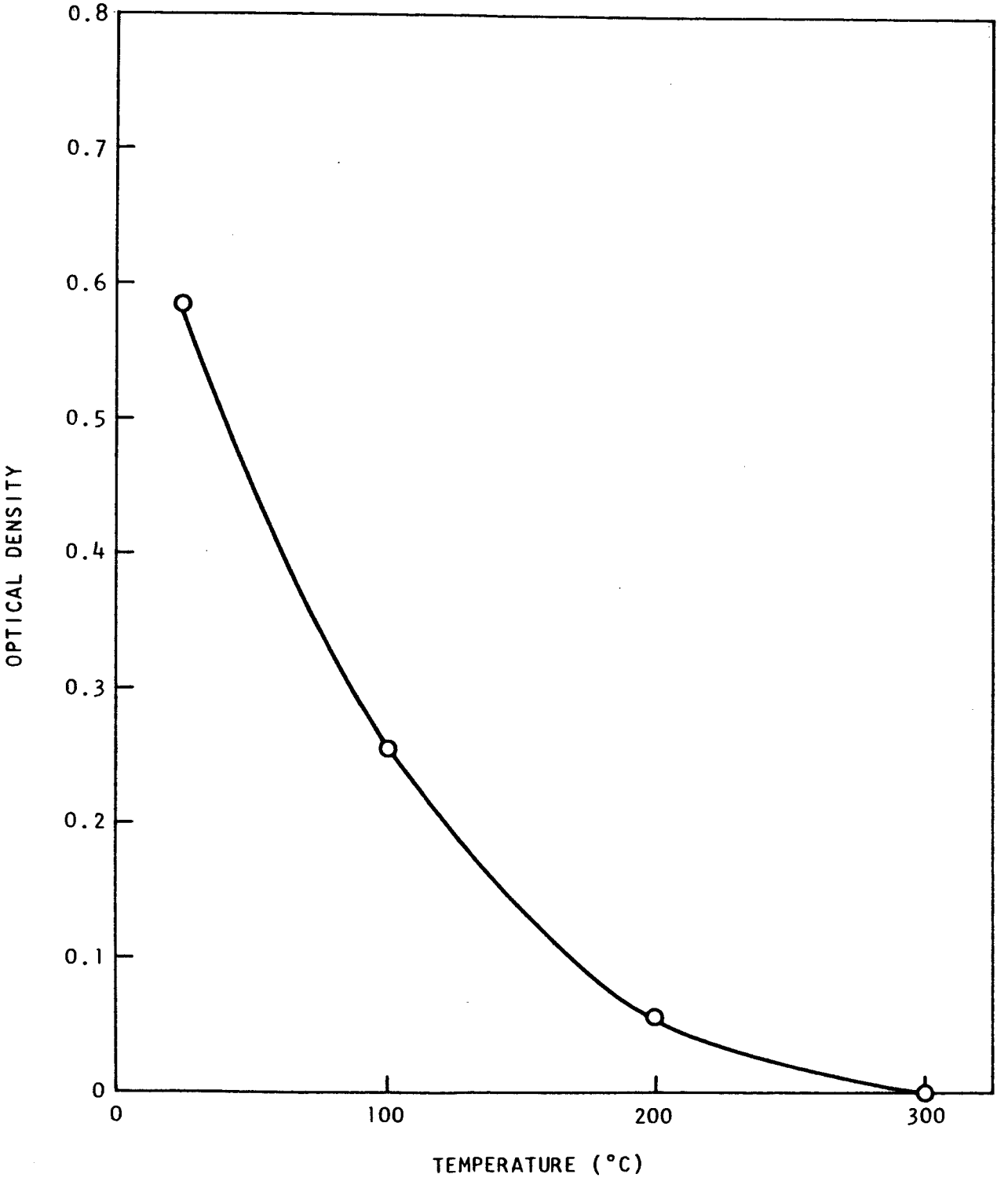

Fig. 36--Optical density at 4, 100 Å of $CaWO_4$:Nd laser rod after γ-ray irradiation and annealing for 30 min at each of the indicated temperatures

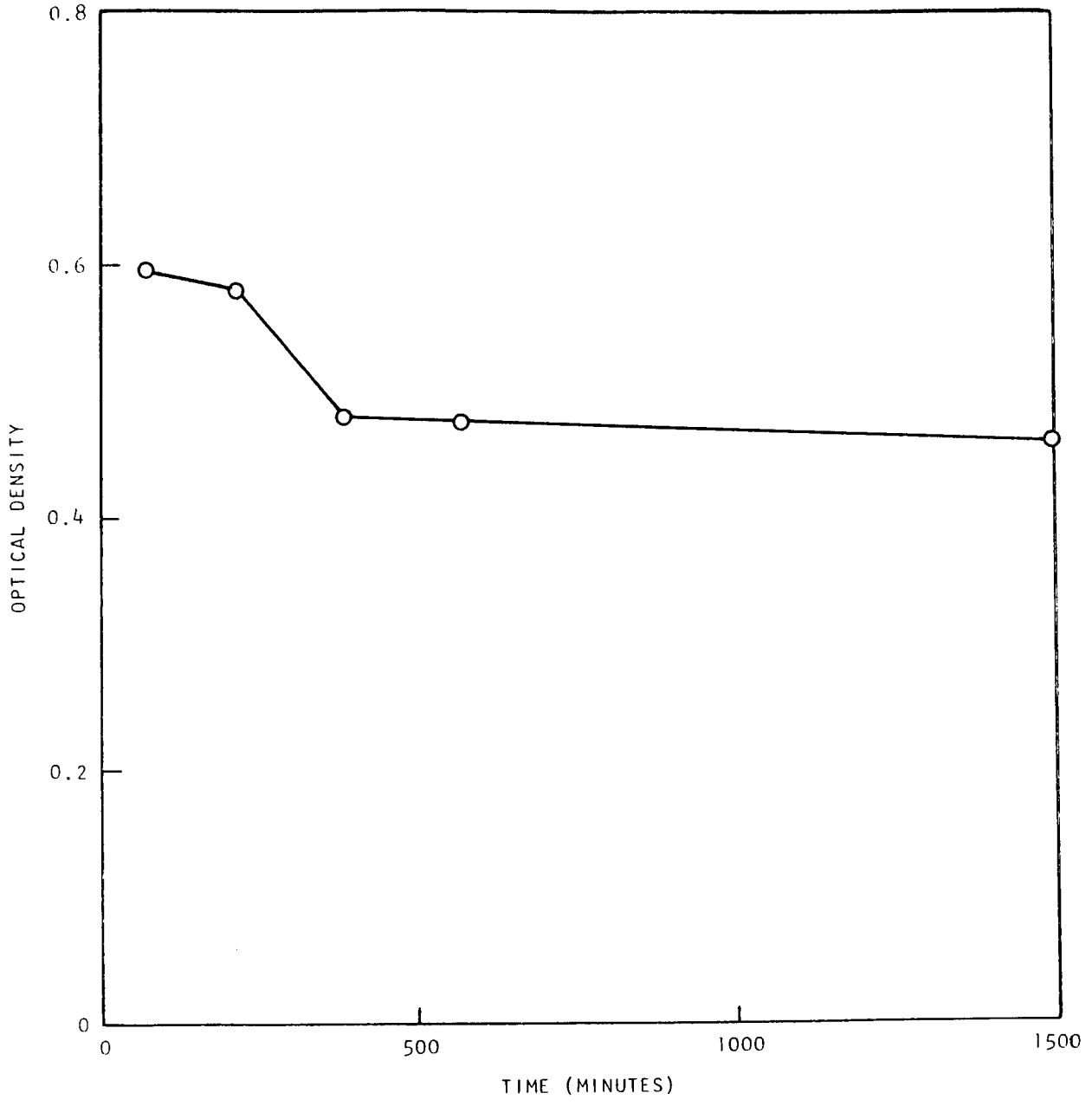

Fig. 37--Decrease of optical density at 4, 100 Å of $CaWO_4$:Nd laser rod as a function of time at room temperature

Apparatus for this purpose was assembled during the reporting period and included a stable light source, a 1.06-μ interference filter, a sample holder into which a laser rod could be precisely positioned, and a phototube using readout by a digital voltmeter to detect changes of 1 part in 10^3 in the transmitted light. It was found very difficult to maintain stability of this order, and only preliminary measurements were made. It is hoped to be able to answer the questions: Is the optical loss which is the source of the effects of irradiation on lasers due only to the optical absorption produced by the irradiation? If not, can it be correlated with the optical absorption? The present indications are that the loss is correlated with absorption, but is higher than can be accounted for by the absorption itself, suggesting some other mechanism, such as scattering by the color centers produced.

4.6 Effects of Different Types of Radiation

Reactor γ rays and electrons with energies in the range 20 to 30 MeV appear to have similar effects on optically pumped lasers when the dosage is expressed in terms of energy deposition (rads). This indicates that the effects are of the ionization type. A comparison with the effects of protons has been handicapped by problems with dosimetry, and more detailed studies require a prior understanding of dose-rate effects.

4.7 Susceptibility to Radiation of Different Laser Rods

Of the three types of Nd-doped laser rods studied, the susceptibility to irradiation appears to increase in the order YAG:Nd; $CaWO_4$:Nd; glass:Nd. Detailed comparisons are not possible at present, because they depend on such factors as how well the laser approaches its theoretical performance before irradiation. Using the cavity with external mirrors imposes a penalty on laser rods with poor optical quality. It is expected that measurements on rods with mirrors directly evaporated on the ends will overcome this.

4.8 Effects on GaAs Lasers

Some preliminary measurements were made on a GaAs injection diode laser. After exposure to 4×10^{11} 30 MeV electrons/cm^2, it was noted that the current versus voltage curve was unchanged, while the light output versus forward current curve showed a drop. In addition, a measurement of output energy versus wavelength showed the appearance of a new emission line. However, these data were taken on a diode that did not show good characteristics (mode structure, etc.) before irradiation, and will not be further discussed here, since greatly improved results, showing the same general features, were obtained on diodes studied after the end of this reporting period. Data on these will be given in a later report.

REFERENCES

1. W. Flowers and J. Jenney, Proc. IEEE 51, 858 (1963).
2. V. R. Johnson and R. W. Grow, Proc. IEEE 52, 185 (1964).
3. W. R. Davis, A. C. Menius, Jr., M. K. Moss, and C. R. Philbrick, J. Appl. Phys. 36, 670 (1965).
4. W. Low, Appl. Phys. Letters 5, 35 (1964).
5. A. F. Gabrysh, H. Eyring, V. LeFebre, and M. D. Evans, J. Appl. Phys. 33, 3389 (1962).
6. R. A. Smith, "Laser Operation in a Neutron and Gamma-ray Field," in First Conference on Laser Technology, San Diego, 1964. (ONR, Washington, D.C. 1964). V. 2, p. 305.
7. V. E. Derr, et al., Crystal Measurements (U), Final Report under Contract AF 33(657)-10489, ASD-TDR-63-740.
8. W. R. Davis, et al., Investigations of the Possibility of Nuclear Driven Laser Systems, Final Report, Contract DA-01-009-ORD-1043, (Oct. 1962).
9. V. R. Johnson and R. W. Grow, Effects of Gamma-Irradiation on the Characteristics of a Ruby Laser, Report NSF-7, (NASA N64-32322), September, 1964.
10. D. M. J. Compton and R. A. Cesena, Effects of Pulsed Irradiation on an Operating Laser (U), General Atomic report GA-6247, April 20, 1965.
11. D. M. J. Compton, J. B. Bryant, R. A. Cesena, and B. L. Gehman, Proc. IEEE 53, 1668 (1965).
12. J. M. Hammer and C. P. Wen, Appl. Phys. Letters 7, 159 (1965).
13. M. Saji and Y. Inuishi, Japan. J. Appl. Phys. 4, 830 (1965).
14. M. C. Petree, Appl. Phys. Letters 3, 67 (1963).
15. M. F. Millea and L. W. Aukerman, Appl. Phys. Letters 5, 168 (1964).
16. M. F. Millea and L. W. Aukerman, J. Appl. Phys. 37, 1788 (1966).
17. A. J. Cohen, Phys. Chem. Solids 13, 321 (1960).

18. D. L. Wood, ibid, 326.

19. J. E. Wertz, et al., J. Phys. Soc. Japan 18, Suppl. II, 305 (1963).

20. M. E. Wyatt, V. A. J. van Lint, and E. G. Wikner, Proton Correlation Studies, Final Report on Contract AF 33(615)-1715 (Technical Report AFML-TR-66-77), General Atomic report GA-6953, April 1966.

21. D. Pooley, Proc. Phys. Soc. (London) 87, 245, 257 (1966).

22. W. Rindnes, H. Roth, and W. Bernard, J. Appl. Phys. 36, 3625 (1965).

23. E. Sonder and W. A. Sibley, Phys. Rev. 129, 1578 (1963).

24. D. M. J. Compton, Optical Studies of Radiation Damage Properties, Final report on Contract AF 19(628)-2926, General Atomic report GA-7140 (to be published).

25. W. T. Roberts, Space Radiations, A Compilation and Discussion, NASA TMX-54700, (Jan. 1964).

26. The Physics of Solar Flares, AAA-NASA Symposium, NASA-SP-50, (Oct. 1963).

27. W. W. Webber, An Evaluation of the Radiation Hazard Due to Solar Particle Events, Boeing Co., Rpt D2-90469 (Nov. 1963).

28. G. D. Magnuson and A. W. McReynolds, Space Electron Shielding-Bremstrahlung and Electron Transmission, General Dynamics report GDA-EPR-AN-617 (February, 1965).

29. C. P. Jupiter and G. Merkel, Bull. APS Series II, 11, 745 (1966).

30. Oak Ridge National Laboratory conducts a "Shielding Newsletter".

31. M. J. Beran and G. B. Parrent, Jr., Theory of Partial Coherence (Prentice-Hall, Inc., Englewood Cliffs, New Jersey, 1964).

32. M. Born and E. Wolf, Principles of Optics (Pergamon Press, New York, 1959).

33. N. R. Kilcoyne, A Study of the Focusing and Collimation Properties of the Pulsed Multi-moding Ruby Laser, AD 460461, Ohio State University report 1579-19, report on Contract AF 33(657)-10824, December 31, 1964 (and references therein).

34. G. B. Parrent and J. J. Skimmer, Optica Acta 8, 93 (1961).

35. C. M. Kellington and M. Katzman, J. Appl. Phys. 36, 2910-2914 (1965).

36. A. Yariv, "Theory of Power Output and Optimum Coupling in Laser Oscillators," in Quantum Electronics, Proceedings of the Third International Congress, ed. by P. Grivet and N. Bloembergen (Columbia University Press, New York, 1964), p. 1055